Spectral Response Function Comparability Among 21 Satellite Sensors for Vegetation Monitoring

Alemu Gonsamo and Jing M. Chen

Abstract—**Global and regional vegetation assessment strategies often rely on the combined use of multisensor satellite data. Variations in spectral response function (SRF) which characterizes the sensitivity of each spectral band have been recognized as one of the most important sources of uncertainty for the use of multisensor data. This paper presents the SRF differences among 21 Earth observation satellite sensors and their cross-sensor corrections for red, near infrared (NIR), and shortwave infrared (SWIR) reflectances, and normalized difference vegetation index (NDVI) aimed at global vegetation monitoring. The training data set to derive the SRF cross-sensor correction coefficients were generated from the state-of-the-art radiative transfer models. The results indicate that reflectances and NDVI from different satellite sensors cannot be regarded as directly equivalent. Our approach includes a polynomial regression and spectral curve information generated from a training data set representing a wide dynamics of vegetation distributions to minimize land cover specific SRF cross-sensor correction coefficient variations. The absolute mean SRF caused differences were reduced from 33.9% (20.1%) to 9.4% (6%) for red, from 3.2% (8.9%) to 1% (1.1%) for NIR, from 2.9% (3.6%) to 1.9% (1.6%) for SWIR, and from 7.1% (9%) to 1.8% (1.7%) for NDVI, after applying the SRF cross-sensor correction coefficients on independent top of canopy (top of atmosphere) data for all-embraced-sensor comparisons. Variations in processing strategies, non spectral differences, and algorithm preferences among sensor systems and data streams hinder cross-sensor spectra and NDVI comparability and continuity. The SRF cross-sensor correction approach provided here, however, can be used for studies aiming at large-scale vegetation monitoring with acceptable accuracy.**

Index Terms—**Cross-sensor comparability, Earth Observing System (EOS) land validation core sites, normalized difference vegetation index (NDVI) continuity, reflectance, spectral response function (SRF).**

I. INTRODUCTION

THE importance of global vegetation in studies of climate, hydrological, and biogeochemical cycles has been well recognized, particularly in carbon studies since plants mediate the land-atmosphere exchange of matter and energy in terrestrial ecosystems [1]. Global, regional, and local vegetation assessment strategies are increasingly incorporating spaceborne remotely sensed information to monitor current and historical vegetation dynamics and often rely on the combined use of multisensor data. Remote sensing makes it possible to collect data from inaccessible and extensive areas with information available in spectral, spatial, angular, geometric, and temporal resolutions and polarization domains with high revisitation frequencies. Although these attributes have largely been a source of additional information, they also hinder the continuity and comparability of multisensor data set which are required for long-term vegetation monitoring due to relatively short life span of satellite sensors.

Since the early 1970s Landsat 1, and the late 1970s launch of the National Oceanic and Atmospheric Administration (NOAA) satellites, the remote sensing communities have accumulated a large amount of invaluable and irreplaceable data set for global vegetation monitoring [2]. The Advanced Very High Resolution Radiometer (AVHRR) sensors, on board of the NOAA satellites, have provided one of the most extensive time series of remotely sensed data and continue producing daily information of surface and atmospheric conditions [3]. Global monitoring of the land surface at coarse spatial resolutions has developed around the use of the AVHRR time series data with predominant use of the normalized difference vegetation index (NDVI), (e.g., [4]–[6]). Several initiatives have been taken to cross calibrate NDVI time series from various sensors all with different purposes and successes: e.g., Pathfinder AVHRR Land (PAL I and II versions) [7], [8], the Global Inventory Monitoring and Modelling Studies (GIMMS) [2], and the Fourier-Adjustment, Solar zenith angle corrected, Interpolated Reconstructed [1], [9]. Despite these efforts, the use of multisensor data for historical monitoring of global vegetations remains a challenge. The main difficulties in the use of multisensor reflective spectra and NDVI time series for operational global vegetation studies arise from differences in: orbital overpass times [10]; geometric, spectral, and radiometric calibration errors [11]–[16]; atmospheric contamination [17], [18]; directional sampling and scanning systems [19], [20] to name a few. The combinations of some of these factors mitigate or exacerbate the resulting variations in solar reflective spectra.

In addition to the aforementioned factors, spectral response function (SRF) variations of different sensors have been recognized as one of the most important factors affecting the continuity of multisensor monitoring of global vegetation [15], [16], [21]–[26]. SRF describes the relative sensitivity of the sensor to monochromatic radiation of different wavelengths and is normally determined in the laboratory using a tunable laser or a scanning monochromator [27]. Differences among the SRF of various radiometers introduce biases that could prevent the detection of reflectance changes resulting from subtle natural variability of vegetation. Teillet *et al.* [15], [16] reported on a radiometric cross calibration of relatively fine spatial resolution sensors to show the spectral band reflectance differences. Teillet

and Ren [24] latter studied spectral band difference effect on NDVI. However, these studies [15], [16] do not provide SRF cross-sensor correction coefficients and are mostly done based on non vegetated land surface spectra. Teillet and Ren [24] do not provide cross-sensor correction coefficients, and the sensitivity analysis is conducted on simulated spectra of limited land cover target types. Trishchenko *et al.* [21] and [23] focused on moderate resolution satellite sensors, including the AVHRR, MODIS, SPOT VEGETATION, and Global Imager all with respect to NOAA9 (N9) AVHRR sensor although the latter study showed SRF differences within the AVHRR-3 series of sensors. They reported on modeling results in the red, near infrared (NIR), and NDVI and provided the difference estimate and polynomial SRF cross-sensor correction coefficients optimized for boreal ecosystems. However, these studies are for limited geographic regions, and the coefficients are provided only in reference to the N9 reference sensor. Trishchenko *et al.* [21] and [23] reported that reflectance differences due to SRF can range from -25% to $+12\%$ in the red and -2% to $+4\%$ in the NIR band, even between "same type" AVHRR series sensors on various NOAA satellites, and that still greater differences can arise for the other sensor intercomparisons. Steven *et al.* [25] provided additional background on the problem of cross cali-brating vegetation indices and reported on a simulation study involving red and NIR spectral bands and vegetation indices for 15 satellite sensors. Rao *et al.* [26] presented results on the cross-sensor correction of MODIS and the European Remote Sensing satellite-2 Along-Track Scanning Radiometer-2 based on desert sites as common targets. They emphasized how crucial it is to take into consideration the spectral characteristics of the sensors and the scene to avoid compromising the effi-cacy of SRF cross-sensor correction. van Leeuwen *et al.* [22] provided extensive sensitivity analysis for SRF cross-sensor correction among MODIS, two AVHRR-2 instruments, and Visible/Infrared Imager Radiometer Suite data from simulated spectra.

The previous studies usually deal with particular sensors which are not necessarily relevant for global vegetation studies or limited for specific geographic regions and land cover types. However, they show important factors affecting the multisensor data uses and comparability and also present detailed sensi-tivity studies such as atmospheric parameters [22]. Practical and operational uses of satellite reflective data to aid our understanding of changing environment must be based on a quantitative appreciation of the biases and uncertainties among different data sources and sensors as specified for example by Global Climate Observing System (GCOS) [28]. GCOS also strongly demands developing satellite-to-satellite cross-calibration algorithms. Therefore, we base our study on the sensitivity analysis of the previous studies with the intention that the general approach for global multisensor SRF cross-sensor correction of bulk spectra can be devised. In such a way, we include most of historically and globally relevant sensors in the last three decades for global vegetation studies and provide differences in reflectances and NDVI, and their SRF cross-sensor correction coefficients. Albeit that most previous studies have focused on NDVI and some with red and NIR reflectances, there is a strong need also to provide SRF cross-sensor correction coefficients for shortwave infrared (SWIR) spectral band. The use of SWIR spectral band in vegetation

studies such as vegetation water content estimations [29] and modifying simple red-NIR ratio index to reduce background and land cover variations in LAI estimation [30] are becoming increasingly indispensable (for example in UofT GLOBCAR-BON LAI and fAPAR algorithms [31]). Therefore, the aim of this study is to evaluate the red, NIR, and SWIR reflectances, and NDVI SRF cross-sensor comparability among 21 satellite sensors, and provide land cover independent SRF cross-sensor correction coefficients for global vegetation monitoring. The SRF cross-sensor corrections are also compared with previous studies applied on an independently measured validation data. The results of this study, previous and ongoing research related to data variations derived from multiple discontinuous sensors, should be of significant value if we are going to be able to make the best informed management decisions and judicious use of the data set.

II. DATA AND METHODS

A. Generation of Synthetic Training Data set

The combined radiative transfer models called PROSPECT for leaf [32], SAIL for canopy [33], and 6 S for atmosphere [18] encoded into Interactive Data Language and Fortran were used to simulate synthetic spectra representing large ranges of possible global vegetation conditions and atmospheric states combined with measured backgrounds and canopy view-sun geometry (Table I). PROSPECT and SAIL are probably the most widely used radiative transfer models in vegetation for developing vegetation indices, and making theoretical sensitiv-ity analysis [34] including SRF cross-sensor correction [22]. The measured background includes most possible scenarios expected in real canopies (Table I). The definitions of all leaf and canopy variables presented in Table I can be found in Jacquemoud *et al.* [35]. In total, 100 spectra were simulated per background type totaling 800 top-of-canopy (TOC) reflectances by combination of the random distribution of the input param-eters bounded by lower and upper bounds (Table I). The lower or upper bounds of the input variables, or the constant setting for some of the variables, were determined based on extensive review of literature for theoretical and measured values (see a review, [34]). The LAI ranges from 0 (consisting only the understorey moss and grass, soil or snow reflectances) to 6 (dense canopy) in order to represent various canopy covers [Fig. 1(a) and (b)]. In addition to this, the lower LAI values also provide spectra consisting of mixed background (green, soil and snow)-vegetation components.

The 6 S radiative transfer model [18] which allows to ac-curately resolve all spectral features of the targets and sensor SRF at 2.5 nm wavelength increments was employed for sim-ulation of signals at satellite level under various atmospheric conditions. Assuming that the surface is of uniform Lambertian reflectance and the atmosphere is horizontally uniform and variable with time, the measured quantities expressed in terms of equivalent reflectance, ρ_{TOA} defined as apparent or top-of-atmosphere (TOA) reflectance was calculated as

$$\rho_{\text{TOA}}(\theta_s, \theta_v, \phi_s - \phi_v)$$

$$= T_g(\theta_s, \theta_v) \left[\rho_{\text{r+a}} + \frac{\rho_t}{1 - S\rho_t} \right] T(\theta_v)T(\theta_s) \quad (1)$$

TABLE I
RANDOM PARAMETER SETS APPLIED TO SIMULATE SYNTHETIC TRAINING DATA USING PROSPECT + SAIL + 6 S RADIATIVE TRANSFER
MODELS INDICATED BY LOWER (LB), UPPER BOUNDS (UP), AND DISTRIBUTIONS. NO BRDF EFFECT WAS CONSIDERED

Variables	Definitions	LB	UB	Distribution
Leaves				
N	Leaf structure parameter	1	2.5	Uniform
C_{ab} (μg.cm^{-2})	Chlorophyll a+b content	20	100	Uniform
C_{dm} (mg.cm^{-2})	Dry matter content	0.025	0.1	Uniform
C_{bp}	Brown pigments content	0.25	0.75	Uniform
C_c (μg.cm^{-2})	Carotenoids content	5	5	Constant
C_w (mg.cm^{-2})	Equivalent water thickness	0.025	0.1	Uniform
ANG	Range of angle of incoming light	5	5	Constant
Canopy				
LAI (m^2.m^{-2})	Leaf area index	0	6	Uniform
LIDF	Leaf inclination distribution function	Spherical	Spherical	Constant
Layer	Number of homogeneous canopy layers	1	1	Constant
Comp	Number of canopy materials	1	1	Constant
Woody	Woody element	0	0	Constant
Diff	Ratio of diffuse to total incident radiation	0.15	0.15	Constant
Canopy view-sun geometry				
Θv(°)	Viewing zenith angle	0	45	Uniform
θs(°)	Solar zenith angle	0	45	Uniform
ϕ_v- ϕ_s(°)	Relative azimuth angle	0	180	Uniform
Background				
Green background				2 samples
Agricultural soil				2 samples
Forest soil				2 samples
Snow				2 samples
Atmosphere				
C_{H2O} (g.cm^{-2})	Water vapour concentration	0.419, 1.42, 4.12		Regular
C_{O3} (DU)	Ozone concentration	247,344, 480		Regular
AOD$_{550nm}$	Aerosol optical depth	0.06	0.06	Constant
Aerosol model		Continental	Continental	Constant
Atmosphere view-sun geometry				
Θv(°)		0	0	Constant
θs(°)		45	45	Constant
ϕ_v- ϕ_s(°)		0	0	Constant

Atmospheric pressure and temperature are derivative of CH2O and CO3. The three atmospheric cases used represent two extreme and one common profiles of atmosphere: US62, Tropical, and Sub-arctic winter.

where θv is view zenith angle, θs is sun zenith angle, ϕ_v is view azimuth angle, ϕ_s is sun azimuth angle, T_g is total gaseous transmittance, ρ_{r+a} is intrinsic atmospheric rayleigh and aerosols reflectance, ρ_t is reflectance of the target, S is spherical albedo of the atmosphere, $T(\theta_v)$ is the total transmittance factor combining the contribution of aerosol and rayleigh along the view-target path $(e^{-\tau/\cos(\theta v)} + E_{sol}^{diff}(\theta v)/\cos(\theta v)E_S)$, $T(\theta_s)$ is total transmittance factor combining the contribution of aerosol and rayleigh along the sun-target path $(e^{-\tau/\cos(\theta s)} + E_{sol}^{diff}(\theta s)/\cos(\theta s)E_s)$, τ is optical thickness of the atmosphere, Es is the solar flux at the top of the atmosphere, and E_{sol}^{diff} is downward diffuse solar irradiance. The coupling of leaf-canopy-atmospheric radiative transfer models involves simply passing the output leaf reflectance and transmittance of the PROSPECT model into the SAIL model to simulate the TOC and using these values as ρ_t in (1) to simulate TOA reflectances using 6 S. The measured background reflectances are used as input to the combined model of PROSPECT, SAIL, and 6 S. This kind of coupling of three radiative transfer models is scarce in literature [35].

We have carried out the 6 S simulations for a standard sun-target-sensor geometry, i.e., $\theta v = 0°$, $\theta s = 45°$, $\Delta\phi$(relative azimuth angle) $= 0°$. This view-target-sun geometry is selected based on previous studies [21], and is a typical geometry to normalize satellite observations [36]. The analysis presented here is limited to a single view-target-sun geometry in 6 S simulations since the simulations were carried out for

an idealized Lambertian surface (angularly uniform reflectance) even though they involve different path lengths through the atmosphere [14], [21]. Above and beyond, the 6 S is parameterized for horizontally uniform atmospheric profiles providing a plane parallel atmosphere whose effect on SRF would be only the extended path length for higher zenith angles. A discussion of the effect of view-target-sun geometry in cross-sensor corrections can be found in [15]. It should be noted that view-target-sun geometry will have effect in SRF cross-sensor correction if real satellite measurements are used as training data due to the anisotropic scattering and transmittance properties of the atmosphere.

The 6 S was run for three typical atmospheric profiles namely: US62 [column integrated water vapor concentration $(C_{H2O}) = 1.42$ g/cm^2 and column integrated ozone concentration $(C_{O3}) = 344$ Dobson units (DU)]; subarctic winter $(C_{H2O} = 0.419$ g/cm^2 and $C_{O3} = 480$ DU); and tropical $(C_{H2O} = 4.12$ g/cm^2 and $C_{O3} = 247$ DU) atmospheres. The atmospheric aerosol optical depth (AOD) has weak wavelength dependence within the considered spectral regions [14], and so it is not expected to play a significant role in the variations of SRF (e.g., [22]). Additionally, optical satellite measurements for surface properties usually employ clear-sky composites selected for the highest atmospheric transparency; therefore, the AOD was set to 0.06 [21], [37]. Our aim here is to provide the bulk cross-sensor correction coefficients to avoid extensive sensitivity analysis; therefore, all the parameter sets are optimized
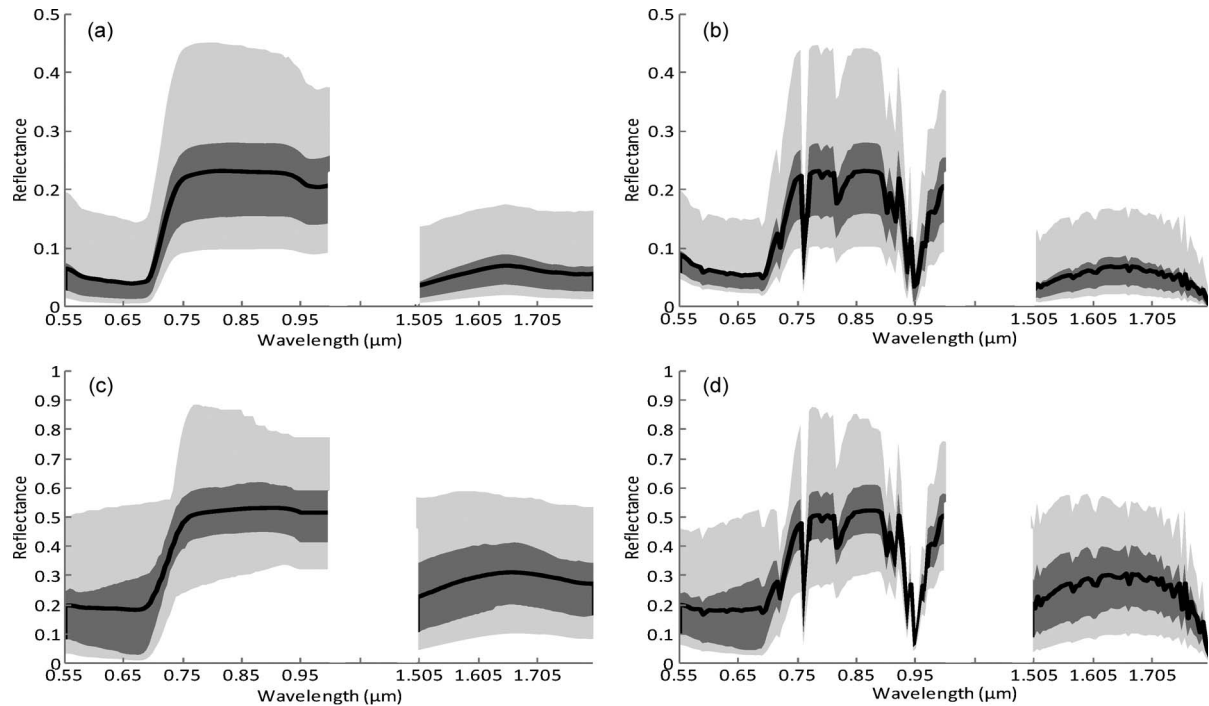
Fig. 1. (a) Synthetic top-of-canopy (TOC) data simulated using PROSPECT and SAIL reflectance models, (b) synthetic top-of-atmosphere (TOA) data simulated using PROSPECT, SAIL, and 6 S radiative transfer models for commonly used US62, subarctic winter and tropical atmospheric profiles, (b) measured TOC data, and (d)TOA data generated from the measured TOC data and 6 S radiative transfer model for US62 atmospheric profile. Bold lines show the average reflectances, the dark gray areas show the bounds between 75% and 25% percentiles, and the light gray areas show the bounds between 95% and 5% percentiles. The data from (a) and (b) are used to generate spectral response function (SRF) cross-sensor correction coefficients whereas the data from (c) and (d) were used to validate the SRF cross-sensor correction performances.

to be relevant for SRF and representative for possible scenario of measured satellite data for global vegetation monitoring. In total, 2400 spectra have been simulated at 2.5 nm spectral intervals using the measured ground backgrounds and coupling PROSPECT + SAIL + 6 S radiative transfer models to synthesize a data set for developing SRF cross-sensor correction coefficients.

B. Measured Ground Data

The preprocessing of satellite data involves many steps in order to be able to obtain the physical value of the surface reflectance without perturbation. Some of these preprocessing can be done quite accurately. Nonetheless, most of them may carry unknown uncertainties due to limited knowledge of input information. Therefore, it is often a challenge to do the training and validation exercise on measured satellite data for SRF cross-sensor corrections. To this regard, several studies have implemented the SRF cross-sensor correction on fully or partially synthetic simulated spectra (e.g., [22]), on ground measured spectra; or airborne imaging spectrometer measurements [21], [23]. The airborne imaging spectrometer data are preferable; however, such measurements are limited and do not represent various conditions of global vegetations. Therefore, we have compiled freely available TOC ground measurements from various time periods, instruments, measurement uncertainties, and locations to be used as independent validation data (Table II). These "bulk" data set are collected using various field spectrometers, accuracies, and field conditions representing large range of plant communities therefore assumed to be reasonable independent validation data set [Fig. 1(c) and (d)]. The data set listed in Table II have been extensively used for

TABLE II
MEASURED TOP-OF-CANOPY VALIDATION DATA FROM
VARIOUS LAND COVER COMMUNITIES

Source	Cover type	Number of spectra
ASTER v2 spectral library	Various soils, vegetations, and snow covers	12
USGS spectroscopy library v splib06a	Various broad-leaf and needle-leaf forest communities	26
Seedling Canopy Reflectance Spectra, 1992-1993 (ACCP)	Tree seedling communities	12
ASD Field Spectrometer Reflectance, Barton Bendish, UK, 1997, 1999, 2000	Various agricultural crop communities	44
SAFARI 2000	Sua Pan salt playa grassland communities	20

devising spectral bands for vegetation structural and biochemical properties, evaluating the sensitivity of vegetation indices, for spectral unmixing, and spectral validation of various sensors to mention a few. The main limitation of the validation data is that there are not many publicly available plant communities TOC data set (note that there are many pure leaf spectra measurements unlike canopy spectra measurements). We have included all the available TOC data, representing wide varieties of plant communities for which the spectral range was found to cover the entire sensor systems considered in this study. The distribution of the plant communities and their background (soil

and snow reflectances) are kept to approximate the real global vegetation distribution scenario.

Table II lists the TOC field measurements used as validation data sets. The ASTER spectral library consists of various materials' spectral compilations from NASA's Jet Propulsion Laboratory, Johns Hopkins University, and the U.S. Geological Survey (USGS—Reston). Among the available spectra, we have chosen those which are relevant for our study such as soils possible in agricultural and forest ecosystems, and TOC reflectances of green grass, conifer, and deciduous plant communities and fine, medium, and coarse granular snow measurements [38]. From the USGS spectral library dry and green TOC reflectance measurements from various grasses, conifers and deciduous vegetation were included in the validation data set [39]. Seedling Canopy Reflectance Spectra, 1992–1993, together with detailed canopy and leaf biochemical and structural properties have been collected for monospecific canopies formed from Douglas-fir (*Pseudotsuga menziesii*) and bigleaf maple (*Acer macrophyllum*) seedlings as a part of NASA's Accelerated Canopy Chemistry Program (ACCP) [40]. These ACCP measurements were also included into the validation data sets. The Analytical Spectral Device (ASD) Fieldspec Pro spectroradiometer measurements at Barton Bendish, UK, 1997, 1999, 2000 were collected from a field site in Hill Farm, Barton Bendish, Norfolk (52.62 N 0.54 E), which is a MODIS core validation site. The Barton Bendish measurements of winter wheat were also included in the validation data sets, measured in several fields using an ASD held at 1 m above the canopy top at 30 m intervals along a transect diagonal to the row direction within each field in order to characterize within-field variability which can arise as a result of variable soil quality and uneven irrigation and application of fertilizer. SAFARI 2000 Sua Pan salt playa grass land communities in the Magkadigkadi region of Botswana was collected from August 18 to September 4, 2000, during the SAFARI 2000 Dry Season Aircraft Campaign using ASD spectroradiometer as a part of MISR validation activities [41]. Each SAFARI 2000 grassland spectra comprises a mean reflectance value over 1 km^2 area, where the mean represents the average of 570 measurements taken over the 1 km^2 area.

C. Measured Satellite Data

To further evaluate the SRF cross-sensor correction results, we compared two sets of data over an Earth Observing System (EOS) land validation core site centered on 42.5° latitude and −72.2° longitude. The site is called Harvard Forest and selected among the other EOS sites due to its predominantly Broadleaf Forest biome which shows seasonal variations on land cover phonology which is assumed to test our SRF cross-sensor correction on various land cover types and photosynthetic biomass amount. The area is approximately 160 by 160 km after truncating the western 40 km pixel width from the standard EOS site due to non vegetated pixels which were replaced with differing data filling algorithm. In addition to this, all the overlapping filled values on low-quality NDVI pixels were ignored from the comparison.

The first data set is the 10-day VGT1 and VGT2 synthesis (S10), a full-resolution (1 km resolution) maximum-value composite (MVC) NDVI product. The VGT1 and VGT2 have an equator-crossing time of 10:30 A.M. local time. Full atmo-

spheric correction is performed correcting for molecular and aerosol scattering, water vapor, ozone, and other gas absorption using measured input data sets such as AOD, subatmospheric C_{H2O}, C_{O3}, and digital elevation model for atmospheric pressure estimation. The S10 NDVI is compiled from VGT1 until January 2003 and VGT2 after that. The SRF of the spectral bands of VGT1 and VGT2 are not identical [Fig. 2(a) and (b)].

The second data set is 16-day composite from the Terra MODIS (MD) 1 km NDVI product (MOD13A2, collection 5) which is based on the MODIS level 2 (L2G) daily surface reflectance product (MOD09 series). The MODIS data is fully corrected for atmospheric scattering and absorption from atmospheric gases, thin cirrus clouds and aerosols. MODIS crosses the equator at 10:30 A.M. local time. The MODIS NDVI compositing algorithm consists of three components: bidirectional reflectance distribution function composite (BRDF-C), constrained-view angle-MVC, and finally if there are not enough "good" observations, MODIS uses MVC. The MVC-based approach prefers the off-nadir views in the forward scatter direction which under clear atmospheric conditions results in higher NDVI values due to relatively darker vegetation shadows in red than NIR band observed in this direction.

D. Satellite Sensors

Twenty-one Earth observation satellite sensors relevant for historical and global study of vegetation were considered (Table III lists the sensor systems, their acronyms, and overall characteristics). The main criterion for sensor selection was the coarser spatial resolution satellites for global vegetation studies. However, we have also included the Landsat 5 TM and 7 ETM+ due to being best understood sensors for their radiometric performances and historic importance [42]. SRFs for each sensor systems were obtained from various sources such as: the operator's website, personal communication, and values tabulated in the 6 S atmospheric correction code. As shown in Fig. 2(a)–(c), [21], and [23], even identical instruments such as AVHRR-3 series sensors on NOAA-15 to 19 and on MetO-A satellites have different SRFs. Therefore, it is important to cross calibrate all the relevant sensors. The quasi-identical sensor systems which are replica of the same instrument such as: AVHRR-1 (N6, N8, N10); AVHRR-2 (N7, N9, N11, N12, N14), Landsat (5 TM, 7 ETM+), SPOT VEGETATION (VGT1, VGT2) are expected to have negligible SRF effects among each other.

E. Methods

The sensor-specific band SRF were used to convolve the simulated training data in order to reproduce the TOC (PROSPECT + SAIL) and TOA (PROSPECT + SAIL + 6 S [US62, Tropical, and Subarctic winter atmospheres]) reflectances for red, NIR, SWIR bands, and NDVI ([NIR-red]/[NIR + red]) for all of the sensor systems considered in this study. These training data were used to derive SRF cross-sensor correction coefficients for both TOC and TOA using ordinary least squares regression models of various forms

$$y_{\text{red,NIR}} = \beta_0 + \beta_1 x_{\text{red}} + \beta_2 x_{\text{NIR}} + \beta_3 x_{\text{NDVI}} + \beta_4 x_{\text{NDVI}^2} + \varepsilon$$
$$y_{\text{NDVI}} = \beta_0 + \beta_1 x_{\text{NDVI}} + \beta_2 x_{\text{NDVI}^2} + \varepsilon$$
$$y_{\text{SWIR}} = \beta_0 + \beta_1 x_{\text{SWIR}} + \varepsilon \tag{2}$$
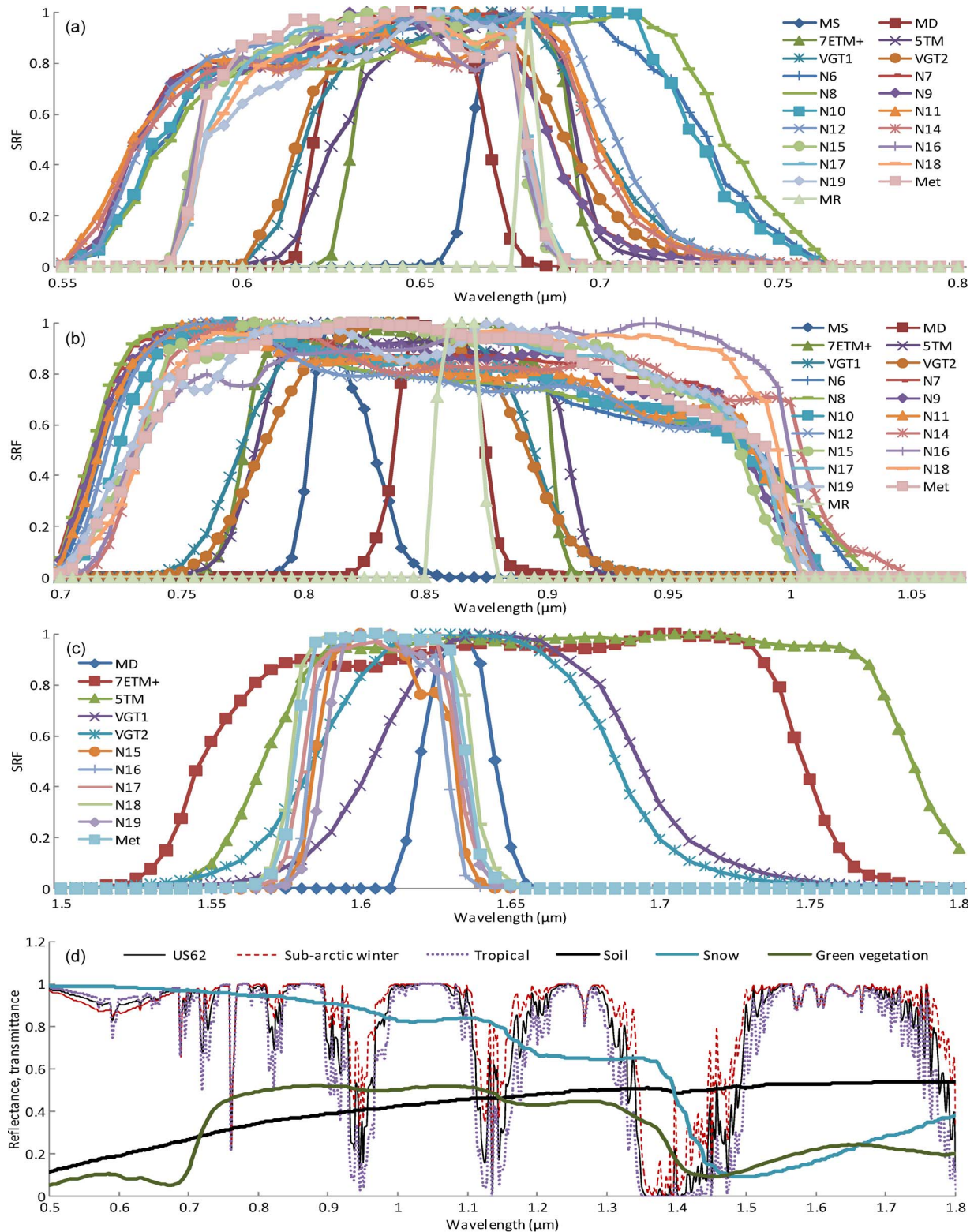
Fig. 2. Spectral response function (SRF) of (a) red, (b) near infrared, and (c) shortwave infrared spectral bands for 21 satellite sensors. (d) Examples of atmospheric transmittance for commonly used US62, subarctic winter and tropical atmospheric profiles, and typical spectral curve of green vegetation, soil, and snow reflectances.

where y and x are the dependent and independent reflectance or NDVI values from two different sensors, respectively. β_0 is the intercept, $\beta_1 - \beta_4$ are the slopes of different independent variables, and ε is unexplained residual error of the model. Examination of the regression analysis shows that the conversion coefficients from a sensor y to sensor x are not exactly the inverse of the coefficients from sensor x to sensor y. The differences arise from residual errors (ε) of the regression; therefore, coefficients are provided for the regression analysis of x versus y and y versus x despite the

TABLE III
LIST OF SELECTED SATELLITE SENSORS AND THEIR CHARACTERISTICS BASED ON
THEIR HISTORIC SIGNIFICANCE FOR GLOBAL VEGETATION MONITORING

ID	Sensor	Functional period	Global repeat coverage	Nominal in–band wavelength (µm)			Nominal pixel size (km)
				Red	NIR	SWIR	
5TM	Landsat 5 TM	1984–present	16 days	0.63–0.69	0.76–0.90	1.55–1.75	0.03
7ETM+	Landsat ETM+	1999–present	16 days	0.63–0.69	0.78–0.90	1.55–1.75	0.03
VGT1	SPOT VEGETATION 1	1998–present	Daily	0.61 – 0.68	0.78 – 0.89	1.58 – 1.75	1.09 – 6.9
VGT2	SPOT VEGETATION 2	2002–present	Daily	0.61 – 0.68	0.78 – 0.89	1.58 – 1.75	1.09 – 6.9
MS	MISR	1999–present	9 days	0.66 –0.682	0.846–0. 886	—	0.250–1.1
MR	MERIS	2002–present	3 days	*0.67–0.69	*0.86–0.88	—	0.3–1.2
MD	MODIS TERRA	1999–present	2 days	0.62 –0. 67	0.841 –0.876	1.628 – 1.652	0.25–1
N6	NOAA 6	1979–1986	Daily	0.58– 0.68	0.725–1.1	—	1.1–6
N7	NOAA 7	1981–1986	Daily	0.58– 0.68	0.725–1.1	—	1.1–6
N8	NOAA 8	1983–1985	Daily	0.58– 0.68	0.725–1.1	—	1.1–6
N9	NOAA 9	1985–1994	Daily	0.58– 0.68	0.725–1.1	—	1.1–6
N10	NOAA 10	1986–1991	Daily	0.58– 0.68	0.725–1.1	—	1.1–6
N11	NOAA 11	1988–2004	Daily	0.58– 0.68	0.725–1.1	—	1.1–6
N12	NOAA 12	1991–2007	Daily	0.58– 0.68	0.725–1.1	—	1.1–6
N14	NOAA 14	1994–2007	Daily	0.58– 0.68	0.725–1.1	—	1.1–6
N15	NOAA 15	1998–present	Daily	0.58– 0.68	0.725–1.1	1.58–1.64	1.1–6
N16	NOAA 16	2000–present	Daily	0.58– 0.68	0.725–1.1	1.58–1.64	1.1–6
N17	NOAA 17	2002–present	Daily	0.58– 0.68	0.725–1.1	1.58–1.64	1.1–6
N18	NOAA 18	2005–present	Daily	0.58– 0.68	0.725–1.1	1.58–1.64	1.1–6
N19	NOAA 19	2009–present	Daily	0.58– 0.68	0.725–1.1	1.58–1.64	1.1–6
Met	MetOp-A	2007–present	Daily	0.58– 0.68	0.725–1.1	1.58–1.64	1.1–6

Present is as of August, 2010. *Among several MERIS spectral bands available in both red and NIR regions, the ones selected here are based on previous study for NDVI production [46] and suitability for vegetation study based on Fig. 2d red-edge distance and atmospheric transmittance

fact that the sensitivity analysis are shown only for the y versus x.

The rationale behind using red, NIR, NDVI, and $NDVI^2$ as independent variables for red and NIR SRF cross-sensor corrections comes from the expected effect of variability of land cover types and optical thickness of the photosynthetic biomass on SRF cross-sensor corrections. Trishchenko *et al.* [21] has demonstrated that the variations of red, NIR, and NDVI between two pairs of sensors with varying SRF are in the order of $NDVI^2$, while NDVI itself partially explains the magnitude of SRF effect and the spectral shape of red and NIR band over vegetated land cover. Other studies [43] have demonstrated that SRF cross-sensor correction is land cover dependent. However, land cover is a dynamic phenomenon particularly in seasonally changing vegetation covers such as temperate and tropical deciduous forests, agricultural lands, and forests in northern and southern hemisphere where the land might be dominated by snow cover in winter times. Thus, providing land cover specific SRF cross-sensor correction coefficients is not practical for operational use. The inclusion of both red and NIR for SRF cross-sensor correction of red and NIR reflectances provides additional information in the regression model about the land cover type, and its effect on the spectral curve. NDVI alone would have provided information about land cover nevertheless soils may have similar NDVI with sparsely vegetated land cover although both respond differently for varying SRF. Moreover, moisture on bare soil and on sparsely vegetated cover may affect differently the relationship between red and NIR if SRF cross-sensor correction is purely based on NDVI variations as used by [21]. Soils, snow, vegetation, and their mixtures are affected differently by varying SRF among sensors [Fig. 2(d)]. The red and NIR reflectance provide added parameters to separate the spectral shape of a range of vegetation or land cover types due to addition information which comes from distance or integration of red-edge region, and various reflectance

responses of distinct cover types in both bands [Fig. 2(d)]. The inclusion for red, NIR, NDVI, and $NDVI^2$ generally characterizes the shape of surface spectra, the magnitude of the SRF effect, the amount of photosynthetic biomass as a result will partially eliminates the need for land cover based SRF cross-sensor correction. The SWIR band on the other hand is mainly affected by leaf water content and less by vegetation structure. The best SRF cross-sensor fit was found by using simple linear regression (2) for SWIR band. NDVI cross-sensor correction of various SRF is slightly affected by land cover types since NDVI by itself partially self cancels perturbation effects. However, NDVI variations are affected nonlinearly by variations of optical thickness of photosynthetic biomass which can be represented by $NDVI^2$ (2) [21]. Above and beyond, it is much worth of use for operational purpose if the NDVI cross-sensor correction coefficients are provided based on solely NDVI itself since most global products do not provide red and NIR reflectance from which the NDVI is derived. In the cases of availability of information on red and NIR bands, the NDVI cross-sensor correction can be made from the SRF cross-sensor corrected red and NIR spectral bands; although only slightly better results were obtained by band cross-sensor correction for NDVI (not presented here).

Finally, the sensor-specific band SRF was used to convolve the measured validation data in order to reproduce the TOC (Table II) and TOA (Table II+ 6 S [US62 atmosphere]) reflectances for red, NIR, SWIR bands, and NDVI for all of the sensor systems considered in this study. For validation data, unlike the training data simulation, only the US62 standard atmospheric profile is chosen due to being the common profile for atmospheric corrections [21], [22], [44]. The regression coefficients for the reflectances and NDVI developed from training data set using (2) are applied on the measured validation data set. The SRF cross-sensor correction fit before and after applying the regression coefficients are

presented for both TOC and TOA databased on mean percent bias ($\Delta\%$) which measures the average disparity between the measurements

$$\Delta\% = \frac{1}{n} \sum_{i=1}^{n} \frac{y_i - x_i}{y_i} * 100 \qquad (3)$$

where y_i and x_i are the two corresponding sensors reflectance or NDVI for the before cross-sensor correction comparison. Moreover, for after cross-sensor correction comparison, the y_i and x_i represent reflectances or NDVI of sensor y with predicted reflectances or NDVI of sensor based on sensor x, respectively.

Finally, we have done extensive literature review for satellite SRF cross-sensor correction in order to make comparisons with previous studies. Although, previous studies are optimized for limited geographic regions and/or land cover types, we have assumed that cross-sensor correction coefficients for NDVI rather than reflectances from these studies could also be applied to our compilations of independent validation data set. NDVI was chosen rather than reflectances because NDVI is assumed to partially remove the limited optimizations of the previous cross-sensor correction coefficients. Only TOC NDVI values were compared since most of the previous studies either solely focus on TOC reflectances [25], [44] or, the TOA NDVI cross-sensor correction coefficients were provided as a function of various atmospheric profiles [21]–[23]. For comparisons with previous studies, the results are rather presented based on the mean absolute difference (MAD), mean bias (Δ), and standard deviation of bias (δ) in order to make them comparable in absolute values with published results

$$\text{MAD} = \frac{1}{2} \sum_{i=1}^{n} |y_i - x_i|.$$

Although important, the scope of this research does not include the combined effects of radiometric calibration accuracy, sensor degradation, detector-specific SRF [45], quality assurance, differences in spatial resolution with view angle [7], atmospheric uncertainty and variability, topography, and sampling directions on SRF of spectral band reflectances and NDVI. The main reason is that this study is aimed at bulk spectra and NDVI cross-sensor correction for global applications, and some of the factors cannot be readily available or measurable in order to include them in the SRF cross-sensor correction regression model. The previous studies have also indicated that the contribution of the aforementioned factors such as atmosphere and view-sun geometry on combined effect of SRF are within $\pm 3\%$ for the reflectance differences (Δ) among several sensors [15], [21]. We have adopted the $\pm 3\%$ relative difference threshold in both reflectances and NDVI to define if the two sensors' measurements are comparable. The $\pm 3\%$ difference among sensors measurements are usually accepted as "good" comparability [15]. Any SRF caused uncertainties within $\pm 3\%$ are comparable to the unseen and uncorrected causes of variations involved in cross-sensor corrections. This hypothesis also implies that SRF cross-sensor correction for reflectance differences within $\pm 3\%$ would not improve the comparability of the two senor measurements. However, we do not recommend ruling out the several corrections if it is possible

at all. To contain some of the factors, we have simulated several atmospheric states and view-target-sun geometry on training data; therefore, the effects should even be further minimized.

In addition to the obvious limitations of the SRF cross-sensor correction among various sensors as discussed in previous sections, there are basic assumptions of SRF cross-sensor correction among instruments as documented in [15] such as: differences in radiometric resolution would not affect the SRF variations; and that the spectral bands were well characterized prior to launch and that they remain unchanged post-launch. The focus in this study is on bulk SRF effects, which could arise regardless of other sources of variations among sensor systems (Section I).

III. CROSS-SENSOR SRF CORRECTION RESULTS

The minimum Pearson correlation coefficient (R) of red $= 0.979(0.979)$, NIR $= 0.998(0.985)$, SWIR $= 0.997(0.996)$, and NDVI $= 0.93(0.93)$, for TOC(TOA), were obtained among any pair of the sensor systems considered among the training data set. This shows that the correlations are not different among the TOC and TOA data set except that the relationships are not $1:1$ (Fig. 3), although no statistical confidence could be inferred from these as the spectral bands of different systems overlap considerably. The intercepts and slopes show substantial differences between the sensors systems that if uncorrected would significantly bias the estimates of any physical products derived from the data set. Among all nominally identical sensor systems, the AVHRR-3 type sensors on N15–N19 and MetOp-A satellites show intercept close to zero and slope close to one with one another indicating the comparability of these sensors. This finding is in good agreement with [21] and [23]. Among these AVHRR-3 sensors, red and SWIR reflectances could be linearly related to one another. Within nominally identical sensor systems, SRF cross-sensor correction of SWIR reflectance has shown consistent slopes and near to zero intercepts (e.g., AVHRR-3 sensors, Landsat sensors, and SPOT VEGETATION sensors).

We have selected MR and N8 sensors to showcase throughout the paper since they consistently revealed the highest disparity in reflectances and NDVI values. The coefficients between TOC and TOA data vary as a result of the distortion by the atmosphere. Fig. 3 shows the scatter plots of these two sensor systems from the training data. The reason for lower red reflectance from MR than from N8 is that the N8's red band SRF involves a considerable amount of wavelength from red-edge region [Fig. 2(a)]. This is opposite for NIR since N8 NIR SRF also extends to the red-edge region for which the reflectance values are relatively smaller than NIR plateau [Fig. 2(b)]. The combined effect results in higher NDVI value from MR than from N8. The impact of the three atmospheric profiles used in the training data can be noted also in TOA results from Fig. 3. The variations due to the three different atmospheric profiles are minor compared to the overall effect of atmosphere on the reflectances and NDVI. The results are higher red reflectance due to higher atmospheric scattering in this wavelength range and lower NIR due to water vapor absorption, resulting in lower overall NDVI. The atmospheric effect on broad band reflectance and SRF is similar with narrow NIR band located around the water vapor window (centered at ~ 0.85 μm) such as MR, MD, and MS sensors.
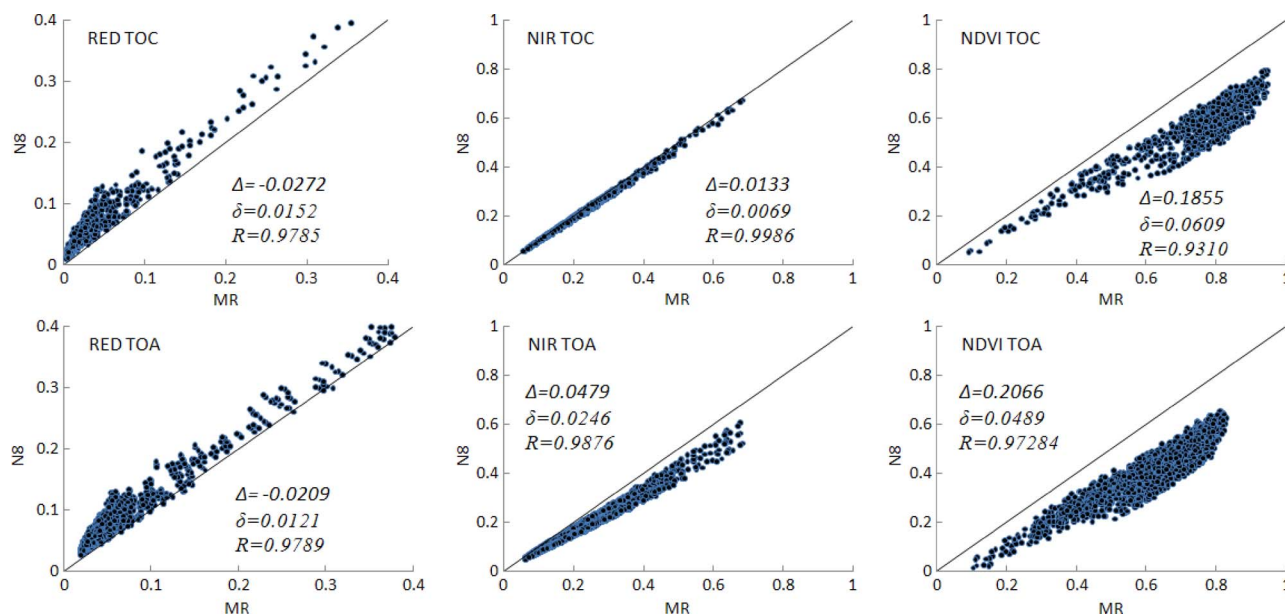
Fig. 3. Variations of red, NIR and NDVI between AVHRR-1 on NOAA-8 satellite (N8) and MERIS (MR) sensor systems from training data for top-of-canopy (TOC) and top-of-atmosphere (TOA) values truncated to the relevant range of vegetation. Diagonal is 1 : 1 line. The mean bias (Δ), standard deviation of the bias (δ), and correlation coefficient (R) between the two sensors are also provided.

IV. VALIDATION RESULTS

Validation of the predicted relationships was performed by comparing the bias reduction obtained after applying the SRF cross-sensor correction coefficients on independent ground measurements. The TOA reflectance from ground measurement is simulated only for the standard US62 base atmosphere unlike the training data which was simulated for two extremes namely tropical and subarctic atmosphere and the US62 profiles. Since, the red reflectances are smaller in value than those of NDVI and NIR, it is important to note that the small difference in red band alone can result in large discrepancies for biophysical parameter estimations. To illustrate the bias of TOC and TOA presented in Tables IV–VII for both before and after SRF cross-sensor correction, we have selected a pair of sensor systems which showed the highest disparity as before (MR and N8) (Fig. 4).

The bias before and after SRF cross-sensor correction is presented in Table IV for red spectral band. The results indicate that all AVHRR-3 instruments (N15, N16, N17, N18, N19, and Met) are comparable to the extent that SRF cross-sensor correction is unnecessary although proportionally large improvement to small differences were observed after the cross-sensor correction. It is expected that these results will be useful for analysis of consistency in the AVHRR time series for the last decade after the launch of NOAA-15 in 1998. In addition, the red, NIR, SWIR, and NDVI also resulted in very small SRF effects in AVHRR-3 sensor systems (Tables IV–VIII). The same result was also obtained by [23] for these sensor systems. Therefore, although the cross-sensor corrections improve the compatibility of the AVHRR-3 sensors, the reflectance and NDVI are deemed to be comparable based on very conservative threshold of ±3% bias. AVHRR-1 and AVHRR-2 have also shown the within ±3% bias reduction after cross-sensor correction when compared with each other. However, the large before-cross-sensor correction bias indicates the cross-sensor correction is necessary among the AVHRR-1 and AVHRR-2

instruments. Unlike AVHRR-1, AVHRR-2 instruments also showed a bias reduction to within ±3% after cross-sensor correction with AVHRR-3 sensors for red spectral band. This is due to progressively smaller overlapping area of the red band and red-edge region from AVHRR-1, to -2, and finally the least overlapping in AVHRR-3 [Fig. 2(a)]. All quasi-identical sensor systems [AVHRR-1 (N6, N8, N10), AVHRR-2 (N7, N9, N11, N12, N14), Landsat (5 TM, 7 ETM+), SPOT VEGETATION (VGT1, VGT2)] have resulted in within ±3% bias among themselves after SRF cross-sensor correction for all the three spectral bands and NDVI (Tables IV–VIII). However, SRF cross-sensor correction is demonstrated to be indispensable among the quasi-identical sensor systems. An overall analysis shows that the SRF caused percent MAD was reduced from 33.9% to 9% and from 20.1% to 6% after applying SRF cross-sensor correction on independent TOC and TOA data, respectively, for all-embraced-sensors comparison of red reflectances. Interesting observation for red spectral band is that, the most narrow band sensors which avoid the red-edge region (i.e., MS, MR, MD), and the most broad band sensors which significantly overlap with the red-edge region (i.e., N6, N8, N10), are the most incomparable sensor systems with others (Table IV). These show that the red-edge is the most important factor for red spectral band cross-sensor correction. Teillet *et al.* [15] also observed similar result for the red band on non vegetated reference surfaces which showed that MS is the most incomparable sensor system. However, even the bias reduction to −10.1% (−0.0015) from −192% (−0.0635) between MR and N8 cross-sensor correction can be considered as a great achievement in such a way making the two instruments comparable (see Table IV and Fig. 4). Overall, bias for red SRF cross-sensor correction presents exaggerated magnitudes in relative terms since differences are divided by smaller values which come from relatively small reflectances of vegetation in red region.

TABLE IV

RED MEAN PERCENT BIAS (AFTER SRF CROSS-SENSOR CORRECTION, BEFORE SRF CROSS-SENSOR CORRECTION). BOTTOM-LEFT LISTS FROM DIAGONAL ARE FOR TOP-OF-CANOPY (TOC) AND TOP-RIGHT LISTS FROM DIAGONAL ARE FOR TOP-OF-ATMOSPHERE (TOA) REFLECTANCES, RESPECTIVELY. DARK GRAY SHADE INDICATES THAT BIAS IS REDUCED TO WITHIN ±3% AFTER SRF CROSS-SENSOR CORRECTION, AND LIGHT GRAY SHADE INDICATES THAT BIAS BEFORE SRF CROSS-SENSOR CORRECTION WAS WITHIN ±3%

	5TM	7ETM+	VGT1	VGT2	MS	MR	MD	N6	N7	N8	N9	N10	N11	N12	N14	N15	N16	N17	N18	N19	Met
5TM		-0.2,4.3	1.8,-16.2	-0.2,-8.3	4.8,10	7.6,9.5	-4.1,0.3	5.3,-60.8	-3.2,-15.1	7.3,-77.6	-3.3,-15	4.9,-57.7	-1.6,-21.2	-1.1,-22.7	-1.8,-19.7	-4.8,-5.5	-4.8,-5.8	-4.6,-4.8	-4.4,-4.4	-4.2,-3.9	-4.7,-5.4
7ETM+	0,7.7		1.8,-21.7	-0.1,-13.3	5.4,6	8.4,5.4	-4.1,-4.3	5.3,-68.7	-3.2,-20.5	7.4,-86.3	-3.3,-20.4	5,-65.4	-1.6,-27	-1.1,-28.5	-1.7,-25.4	-4.8,-10.3	-4.7,-10.6	-4.5,-9.7	-4.4,-9.2	-4.1,-8.6	-4.7,-10.3
VGT1	1.7,-28.3	1.2,-39.9		-1.9,6.7	1.6,22	4.1,21.7	-5.6,13.9	3.4,-37.6	-4.6,0.9	5.3,-51.8	-4.7,1	3.1,-35	-3.1,-4.2	-2.6,-5.4	-3.3,-2.9	-6.1,9.1	-6.3,8.8	-6,9.6	-5.9,9.9	-5.7,10.4	-6.1,9.1
VGT2	-0.6,-13.2	-1.2,-23.1	-2.1,11.3		4.2,16.6	6.8,16.2	-3.8,7.8	5.3,-48	-2.9,-6.2	7.3,-63.3	-2.9,-6.1	5,-45.1	-1.3,-11.8	-0.8,-13.2	-1.5,-10.4	-4.4,2.6	-4.4,2.3	-4.2,3.2	-4.1,3.5	-3.8,4.1	-4.3,2.6
MS	8,18.1	9.4,11.5	2.9,34.7	6.4,27		4.4,-1.8	3.3,-0.6	-10.8,-11.1	-9.6,-28.7	0.9,-99.7	-9.7,-28.6	-1.6,-77.1	-8.1,-35.7	-7.7,-37.4	-8.3,-34	-11.3,-17.7	-11.2,-18	-11.1,-17	-10.9,-16.5	-10.6,-15.9	-11.3,-17.7
MR	11.1,16.9	13,10.1	4.6,33.8	8.7,26	4.4,-1.8		-26.1,-16.6	-14.1,-10.5	-4.1,-79.3	-12.7,-27.9	-12.7,-27.8	-4.4,-75.8	-11.1,-34.8	-10.7,-36.5	-11.3,-33.1	-14.5,-17	-14.4,-17.4	-14.3,-16.3	-14.1,-15.9	-13.8,-15.2	-14.4,-17
MD	-5.8,3.8	-6.6,-4.3	-6.6,23.9	-4.9,14.6	-21.7,-18.5	-26.1,-16.6		9.1,-61.6	0.8,-15.5	11,-78.4	0.7,-15.4	8.7,-58.4	2.4,-21.7	2.9,-23.2	2.2,-20.2	-0.7,-5.8	-0.7,-6.1	-0.4,-5.1	-0.3,-4.7	0,-4.2	-0.6,-5.8
N6	6.3,-105.4	5.7,-125.4	4.2,-57.3	6.6,-79.3	-10,-160.3	-14.1,-154.7	12.5,-115.6		-6.5,27.3	1.5,-10	-6.5,27.3	-0.3,1.9	-5.3,23.7	-4.9,22.8	-5.6,24.6	-7.8,33	-8,32.9	-7.7,33.4	-7.7,33.6	-7.5,34	-7.9,33
N7	-5.3,-20.3	-6.4,-31.1	-5.5,5.9	-4,-6.2	-22.3,-50	-26.3,-47.2	0.3,-25.6	-7,38.4		9.8,-53.3	0,0.1	7.7,-36.4	1.6,-5.2	2.1,-6.5	1.4,-3.9	-1.3,8.2	-1.4,8	-1.2,8.7	-1,9.1	-0.8,9.6	-1.3,8.2
N8	9.6,-134.8	9.2,-158.1	6.9,-79.2	9.6,-104.6	-5.9,-198.5	-10.1,-192	15.9,-146.7	1.9,-13.2	14.2,-91.9		-7.5,33.7	-1.7,10.7	-6.3,30.4	-5.9,29.6	-6.7,31.2	-8.6,38.9	-9,38.7	-8.6,39.2	-8.7,39.4	-8.5,39.7	-8.8,38.9
N9	-5.4,-20.2	-6.5,-30.9	-5.6,6	-4.1,-6.1	-22.4,-49.9	-26.5,-47	0.2,-25.4	-7,38.4	0,0.1	-8,45.1		7.7,-36.5	1.6,-5.3	2.1,-6.6	1.4,-4	-1.3,8.2	-1.4,7.9	-1.1,8.7	-1,9	-0.8,9.5	-1.3,8.2
N10	5.2,-99.6	4.6,-119	3.4,-53	5.7,-74.3	-11.1,-152.8	-15.3,-147.3	11.4,-109.4	-0.5,2.6	10.3,-63.6	-2.2,13.8	10.3,-63.8		-5.2,22.2	-4.7,21.3	-5.5,23.2	-7.7,31.8	-8,31.6	-7.7,32.2	-7.7,32.4	-7.5,32.8	-7.8,31.8
N11	-3.9,-32.1	-5.1,-44.1	-4.2,-2.9	-2.7,-16.3	-21.1,-65.3	-25.2,-62	1.7,-38	-5.9,33	1.6,-9.5	-7,40.4	1.6,-9.6	-5.7,31.3		0.5,-1.2	-0.2,1.2	-2.9,12.7	-3.1,12.4	-2.8,13.2	-2.7,13.5	-2.5,13.9	-2.9,12.7
N12	-3.4,-35.4	-4.5,-47.8	-3.8,-5.3	-2.2,-19.2	-20.6,-69.7	-24.7,-66.2	2.3,-41.6	-5.6,31.5	2.1,-12.1	-6.7,39.1	2.1,-12.3	-5.4,29.8	0.5,-2.4		-0.7,2.4	-3.4,13.7	-3.6,13.4	-3.3,14.2	-3.2,14.5	-3,14.9	-3.4,13.7
N14	-4.1,-29.5	-5.2,-41.3	-4.5,-0.9	-2.9,-14.1	-21.5,-62	-25.6,-58.8	1.6,-35.3	-6.4,34.2	1.4,-7.4	-7.5,41.4	1.4,-7.5	-6.1,32.6	-0.2,1.9	-0.7,4.2		-2.7,11.6	-2.8,11.4	-2.6,12.1	-2.5,12.4	-2.3,12.9	-2.7,11.6
N15	-6.9,-4.8	-7.9,-13.8	-7.1,17.4	-5.6,7.2	-23.7,-29.8	-27.9,-27.5	-1.3,-9.1	-8.4,45.4	-1.7,12.4	-9.3,51.2	-1.7,12.4	-8.2,44.1	-3.2,19.7	-3.6,21.5	-3,18.2		-0.1,-0.4	0,-0.3	0.2,0.6	0.4,1	0.1,0
N16	-7,-5.2	-8,-14.3	-7.3,17.1	-5.8,6.8	-23.8,-30.4	-28,-28.1	-1.3,-9.6	-8.9,45.2	-1.9,12.1	-9.8,51	-1.9,12	-8.7,43.8	-3.5,19.3	-3.9,21.2	-3.2,17.9	-0.1,-0.4		0.3,0.9	0.4,1.2	0.6,1.8	0.1,0.3
N17	-6.5,-3.9	-7.5,-12.8	-6.9,18.1	-5.3,8	-23.1,-28.6	-27.3,-26.4	-0.8,-8.2	-8.3,45.8	-1.5,13.2	-9.3,51.6	-1.4,13.1	-8.2,44.5	-3,20.3	-3.4,22.1	-2.8,18.9	0.4,0.8	0.4,1.3		0.2,0.4	0.4,0.9	-0.2,-0.6
N18	-6.2,-3.2	-7,-12.1	-6.7,18.6	-5.1,8.5	-22.6,-27.8	-26.8,-25.6	-0.4,-7.5	-8.4,46.1	-1.3,13.7	-9.4,51.8	-1.2,13.6	-8.3,44.8	-2.9,20.8	-3.3,22.6	-2.6,19.3	0.7,1.5	0.7,1.9	0.3,0.6		0.2,0.5	-0.3,-1
N19	-5.7,-2.4	-6.5,-11.2	-6.4,19.2	-4.7,9.2	-21.9,-26.7	-26.1,-24.5	0,-6.6	-8.2,46.5	-1,14.3	-9.1,52.2	-0.9,14.3	-8,45.2	-2.6,21.4	-3,23.2	-2.3,20	1,2.2	1.1,2.7	0.7,1.4	0.4,0.8		-0.6,-1.5
Met	-6.9,-4.8	-7.9,-13.9	-7.1,17.4	-5.6,7.2	-23.7,-29.9	-27.9,-27.6	-1.2,-9.1	-8.5,45.4	-1.7,12.4	-9.4,51.2	-1.7,12.3	-8.3,44	-3.2,19.6	-3.6,21.5	-3,18.2	0.1,0	0.1,0.4	-0.3,-0.9	-0.7,-1.5	-1.1,-2.3	

Table V presents the bias before and after SRF cross-sensor correction for TOC and TOA reflectance of NIR spectral band. Unlike the red, NIR was successfully reduced to within ±3% bias after SRF cross-sensor correction for all of the sensor systems considered. Except that of some of N6, N7, and N8 pairs, all AVHRR-1, -2, and -3 resulted in within ±3% bias before SRF cross-sensor correction indicating that these instruments are comparable in NIR spectral band among each other. All of the three narrow band instruments (MS, MR, and MD) and Landsat and SPOT VEGETATION sensor systems have shown "good" comparability among themselves and relatively poor comparability with other AVHRR sensor systems (Table V). NIR reflectance in vegetated landscape is large therefore although the bias seems comparably low relative to results obtained for red band, the SRF cross-sensor correction is advised (Fig. 4) particularly for the TOA reflectance where the transmittance is varying in NIR region [Fig. 2(d)]. For NIR spectral band, the absolute mean SRF caused differences were reduced from 3.2% (8.9%) to 1% (1.1%) after applying the SRF cross-sensor correction coefficients on independent top of canopy (top of atmosphere) data for all-embraced-sensor comparisons.

Table VI presents the before and after SRF cross-sensor correction bias for TOC and TOA NDVI. Like NIR, bias of NDVI which can be compared in relative perspective from Fig. 4 shows relatively smaller values since the differences are divided by large number in contrast to red spectral band. NDVI shows the combined effects of red and NIR sensitivity to SRF variations, although the large discrepancy from red is expected to play a major role. Table VI shows the two least comparable groups, i.e., the relatively narrow and broad band sensor systems which exhibited to be less comparable with other sensor systems in red spectral region as discussed above also propagate this effect into NDVI. The first group includes the sensor systems which significantly overlap the red-edge region in red spectral band [AVHRR-1: N6, N8 and N10, Fig. 2(a)] showing less comparability with other sensors. The second group includes the narrow band sensor systems (e.g.,

TABLE V
SAME AS TABLE IV BUT FOR NIR REFLECTANCES

	5TM	7ETM+	VGT1	VGT2	MS	MR	MD	N6	N7	N8	N9
5TM		0,-1.1	0.1,0	0.1,-0.3	1.5,4.4	-0.2,-7.5	-0.4,-6.1	1.1,15.8	1.8,17.3	1.2,16.8	1.8,16.9
7ETM+	0.1,0		0.1,1.1	0.1,0.8	1.6,5.5	-0.2,-6.4	-0.4,-5	1.2,16.7	1.9,18.2	1.3,17.8	1.9,17.8
VGT1	0.2,0.3	0.1,0.2		-0.1,-0.3	1.5,4.4	-0.3,-7.5	-0.5,-6.1	1.1,15.8	1.8,17.3	1.2,16.9	1.7,16.9
VGT2	0.1,0.1	0.1,0.1	-0.1,-0.2		1.5,4.7	-0.3,-7.2	-0.5,-5.8	1.1,16	1.8,17.6	1.2,17.1	1.8,17.1
MS	1.3,0.5	1.2,0.4	1.1,0.2	1.1,0.4		-0.6,-12.5	-1.1,-11	-0.4,11.9	0.1,13.5	-0.3,13	0.1,13
MR	-1.1,-1	-1.1,-1	-1.3,-1.2	-1.2,-1	-2.4,-1.4		0.1,1.3	2.6,21.7	3.4,23.1	2.6,22.7	3.4,22.7
MD	-0.7,-0.7	-0.8,-0.7	-0.9,-1	-0.8,-0.8	-2,-1.2	0.4,0.3		2.2,20.6	3,22.1	2.3,21.6	3,21.7
N6	-0.4,6.2	-0.5,6.2	-0.6,5.9	-0.6,6.1	-1.7,5.7	0.6,7.1	0.2,6.8		0.2,1.8	0.2,1.3	0.2,1.3
N7	-0.3,6.7	-0.4,6.7	-0.5,6.4	-0.5,6.6	-1.6,6.3	0.8,7.6	0.4,7.3	-0.1,0.5		0,-0.6	0,-0.5
N8	-0.4,7.2	-0.4,7.2	-0.6,6.9	-0.5,7.1	-1.6,6.7	0.7,8	0.3,7.8	0.1,1.1	0.2,0.5		0,0
N9	-0.3,6.4	-0.3,6.3	-0.5,6.1	-0.4,6.3	-1.6,5.9	0.8,7.2	0.4,7	0,0.2	0.1,-0.4	-0.2,-0.9	
N10	-0.5,4.7	-0.6,4.7	-0.7,4.5	-0.6,4.7	-1.8,4.3	0.6,5.6	0.1,5.4	-0.1,-1.5	0,-2.1	-0.2,-2.6	-0.1,-1.7
N11	-0.3,6.3	-0.4,6.3	-0.5,6	-0.4,6.2	-1.6,5.8	0.8,7.2	0.4,6.9	-0.1,0.1	0,-0.4	-0.2,-1	0,-0.1
N12	-0.3,5.8	-0.4,5.8	-0.5,5.6	-0.4,5.7	-1.6,5.4	0.8,6.7	0.4,6.4	0,-0.4	0.1,-1	-0.2,-1.5	0,-0.6
N14	-1.1,3.4	-1.2,3.4	-1.3,3.1	-1.3,3.3	-2.4,2.9	0.4,3	-0.4,4	-0.9,-3	-0.8,-3.6	-1,-4.1	-0.8,-3.2
N15	-0.6,3.8	-0.6,3.7	-0.8,3.5	-0.7,3.7	-1.9,3.3	0.6,4.7	0.1,4.4	-0.4,-2.6	-0.3,-3.2	-0.5,-3.7	-0.3,-2.8
N16	-1.5,3.3	-1.6,3.3	-1.7,3.1	-1.6,3.2	-2.8,2.9	-0.4,4.2	-0.8,4	-1.3,-3	-1.2,-3.6	-1.5,-4.2	-1.3,-3.2
N17	-0.8,3.6	-0.8,3.6	-1,3.3	-0.9,3.5	-2.1,3.1	0.4,4.5	-0.1,4.2	-0.5,-2.8	-0.5,-3.3	-0.7,-3.9	-0.5,-3
N18	-1.1,3.6	-1.2,3.5	-1.3,3.3	-1.2,3.5	-2.4,3.1	0.4,5	-0.4,4.2	-0.9,-2.8	-0.8,-3.4	-1.1,-3.9	-0.9,-3
N19	-0.8,4.2	-0.8,4.1	-1,3.9	-0.9,4.1	-2.1,3.7	0.4,5	-0.1,4.8	-0.6,-2.2	-0.5,-2.7	-0.7,-3.3	-0.5,-2.4
Met	-0.8,3.6	-0.8,3.6	-1,3.3	-0.9,3.5	-2.1,3.2	0.4,4.5	-0.1,4.3	-0.5,-2.8	-0.5,-3.3	-0.7,-3.9	-0.5,-3

	N10	N11	N12	N14	N15	N16	N17	N18	N19	Met
5TM	1.1,14.9	1.5,16.4	1.4,15.9	0.9,14.6	1.4,14.5	1.1,16	1.2,14.5	1.2,15.4	1.3,14.9	1.1,13.9
7ETM+	1.2,15.8	1.7,17.3	1.5,16.8	1,15.6	1.5,15.4	1.3,16.9	1.3,15.5	1.3,16.4	1.4,15.9	1.2,14.9
VGT1	1,14.9	1.5,16.4	1.4,15.9	0.9,14.6	1.4,14.5	1.1,16	1.2,14.5	1.2,15.5	1.3,14.9	1,13.9
VGT2	1.1,15.1	1.6,16.7	1.4,16.1	0.9,14.9	1.4,14.8	1.2,16.3	1.2,14.8	1.2,15.7	1.3,15.2	1.1,14.2
MS	-0.4,11	-0.1,12.6	-0.2,12	-0.8,10.7	-0.2,10.5	-0.6,12.2	-0.4,10.6	-0.5,11.5	-0.3,11	-0.5,9.9
MR	2.5,20.9	3.1,22.3	3,21.7	2.5,20.6	3,20.5	2.9,21.9	2.8,20.5	2.9,21.4	3,20.9	2.7,20
MD	2.2,19.8	2.7,21.2	2.6,20.7	2.1,19.5	2.6,19.4	2.5,20.9	2.4,19.4	2.4,20.3	2.5,19.8	2.3,18.9
N6	-0.1,-1.1	0.1,0.8	0,0.1	-0.6,-1.4	-0.2,-1.6	-0.6,0.3	-0.4,-1.5	-0.5,-0.4	-0.3,-1	-0.5,-2.2
N7	-0.2,-2.9	-0.1,-1.1	-0.2,-1.8	-0.8,-3.3	-0.4,-3.4	-0.8,-1.6	-0.6,-3.4	-0.7,-2.3	-0.5,-2.9	-0.7,-4.1
N8	-0.2,-2.4	-0.1,-0.5	-0.2,-1.2	-0.8,-2.7	-0.4,-2.8	-0.8,-1	-0.6,-2.8	-0.7,-1.7	-0.5,-2.3	-0.7,-3.5
N9	-0.2,-2.4	-0.1,-0.5	-0.2,-1.2	-0.8,-2.7	-0.4,-2.9	-0.8,-1	-0.6,-2.8	-0.7,-1.7	-0.5,-2.4	-0.7,-3.6
N10		0.2,1.8	0.1,1.1	-0.5,-0.3	-0.1,-0.5	-0.5,1.3	-0.2,-0.4	-0.3,0.6	-0.2,0	-0.4,-1.1
N11	0.1,1.6		-0.1,-0.7	-0.7,-2.2	-0.3,-2.3	-0.7,-0.5	-0.5,-2.3	-0.6,-1.2	-0.4,-1.8	-0.6,-3
N12	0.1,1.1	0,-0.5		-0.6,-1.5	-0.2,-1.6	-0.6,0.2	-0.4,-1.6	-0.5,-0.5	-0.3,-1.1	-0.5,-2.3
N14	-0.7,-1.4	-0.8,-3.1	-0.8,-2.6		0.5,-0.1	0,1.6	0.3,-0.1	0.2,1	0.4,0.4	0.2,-0.8
N15	-0.2,-1	-0.3,-2.7	-0.3,-2.2	0.5,0.4		-0.4,1.8	-0.2,0	-0.3,1.1	-0.1,0.5	-0.3,-0.7
N16	-1.2,-1.5	-1.3,-3.2	-1.3,-2.6	-0.4,-0.1	-0.9,-0.4		0.3,-1.8	0.2,-0.7	0.3,-1.3	0.2,-2.5
N17	-0.4,-1.2	-0.5,-2.9	-0.5,-2.4	0.4,0.2	-0.2,-0.2	0.8,0.3		-0.1,1.1	0.1,0.5	-0.1,-0.7
N18	-0.8,-1.2	-0.9,-2.9	-0.9,-2.4	0,0.2	-0.6,-0.2	0.4,0.2	-0.4,0		0.2,-0.6	0,-1.8
N19	-0.4,-0.6	-0.5,-2.3	-0.5,-1.8	0.3,0.8	-0.2,0.4	0.7,0.8	0.0,0.6	0.4,0.6		-0.2,-1.2
Met	-0.4,-1.2	-0.5,-2.9	-0.5,-2.4	0.3,0.2	-0.2,-0.2	0.8,0.3	0,0	0.4,0.1	0,-0.6	

MS and MR) which have the red band far away from the red-edge and NIR band approximately located at atmospheric window away from the red-edge showing less comparability with other sensors (Table VI). However, all of the biases after SRF cross-sensor corrections were within ±3% indicating the regression coefficients can be used for cross-sensor correction of NDVI among all sensor systems. One of the least comparable pairs (i.e., MR and N8) successfully reduced to within ±3% after the SRF cross-sensor corrections. These demonstrate that NDVI which is most commonly used to monitor global vegetation functioning and change can be successfully corrected for cross-sensor SRF differences. The absolute mean SRF caused differences were reduced from 7.1% (9%) to 1.8% (1.7%) for NDVI after applying the SRF cross-sensor correction coefficients on independent top of canopy (top of atmosphere) data for all-embraced-sensor comparisons.

Table VII presents the before and after SRF cross-sensor correction bias for TOC and TOA reflectances of SWIR spectral band. Overall, SWIR is more comparable and less dependent on spectral shape for SRF cross-sensor correction compared to red and NIR spectral bands. All of the AVHRR-3 instruments have relatively comparable SWIR reflectance without SRF cross-sensor corrections. This study has provided the SWIR SRF cross-sensor correction for the first time. Generally speaking, the absolute mean SRF caused differences were reduced from 2.9% (3.6%) to 1.9% (1.6%) for SWIR spectral band after applying the SRF cross-sensor correction coefficients on independent top of canopy (top of atmosphere) data for all-embraced-sensor comparisons.

V. APPLICATION ON REAL SATELLITE DATA

Given the compositing period and method, and other inherent variations (Section I) among the sensor systems, we have post-processed the VGT1, VGT2, and MD NDVI data set for spatial and temporal aggregations. All filled pixels were removed from analysis, and all negative NDVI values were replaced by zero since the data set treat them separately. To reduce the influence of sampling technique including the differences in VGT and MD point-spread function on this specific data sets [47], and spatial resolution on NDVI although the latter is more severe for high resolution sensors [48], we further averaged the NDVI

TABLE VI
SAME AS TABLE IV BUT FOR NDVI

	5TM	7ETM+	VGT1	VGT2	MS	MR	MD	N6	N7	N8	N9
5TM		-0.1,-1.3	0.5,3.8	0.2,1.8	-0.8,-1.1	-1.3,-4.2	0,-1.8	0.3,20.2	0.1,9.6	0.4,24.5	0.1,9.4
7ETM+	0.1,-1.2		0.6,5	0.3,3.1	-0.8,0.3	-1.3,-2.8	0.1,-0.4	0.6,21.2	0.3,10.8	0.7,25.5	0.3,10.6
VGT1	-0.4,4.3	-0.5,5.5		-0.2,-2	-0.8,-5.1	-1.4,-8.3	-0.2,-5.8	-0.3,17.1	-0.3,6.1	-0.4,21.6	-0.3,5.9
VGT2	0,2	-0.1,3.2	0.5,-2.4		-0.8,-3	-1.3,-6.2	-0.1,-3.7	0.1,8.7	-0.2,7.9	0.2,3.1	-0.1,7.7
MS	-0.9,-2.9	-1,-1.7	-0.4,-7.6	-0.9,-5.1		-0.4,-3.1	1.6,-0.8	2.3,21	1.6,10.6	2.3,25.3	1.6,10.4
MR	-1.9,-3.1	-2,-1.8	-1.3,-7.8	-1.8,-5.2	-0.9,-0.1		2.1,2.3	3,23.3	2.6,13.2	3.1,27.5	2.7,13
MD	0.7,-0.7	0.6,0.5	1.3,-5.3	0.8,-2.8	1.8,2.1	2.7,2.3		0.4,21.5	0.1,11.2	0.4,25.8	0.1,11
N6	-1.4,16.8	-1.4,17.7	-1.2,13	-1.5,15	0.1,19.1	1,19.2	-2.2,17.3		0.3,-13.3	-0.2,5.4	0.3,-13.6
N7	0.5,4.6	0.5,5.8	1,0.3	0.6,2.6	1.7,7.3	2.6,7.4	-0.2,5.3	2.5,-14.7		0.4,16.5	0.1,-0.2
N8	-1.9,21	-1.8,21.9	-1.7,17.4	-2,19.4	-0.3,23.2	0.6,23.3	-2.6,21.5		-2.9,17.2		0.6,-20.1
N9	0.5,4.5	0.5,5.7	1,0.2	0.6,2.5	1.7,7.2	2.6,7.3	-0.2,5.2	2.6,-14.8	0,-0.1	3.3,-21	
N10	-1.4,15.5	-1.3,16.5	-1.1,11.7	-1.4,13.8	0.1,17.9	1.1,18	-2.1,16.1	0.1,-1.5	-2.2,11.5	0.8,-6.9	-2.2,11.6
N11	0.2,6.4	0.2,7.5	0.7,2.1	0.2,4.4	1.4,9	2.4,9.1	-0.5,7	2.1,-12.6	-0.4,1.8	2.9,-18.6	-0.4,1.9
N12	0.1,6.8	0.1,7.9	0.6,2.5	0.1,4.8	1.4,9.4	2.3,9.5	-0.6,7.4	2,-12.1	-0.5,2.2	2.7,-18.1	-0.5,2.3
N14	0.5,2	0.6,3	0.5,0.9	0.1,3.2	1.3,7.9	2.2,8	-0.7,5.9	2,-13.9	-0.5,0.6	2.7,-20.1	-0.6,0.7
N15	0.8,1.5	0.7,2.7	1.3,-3	0.9,-0.5	1.9,4.3	2.9,4.4	0.1,2.2	2.9,-18.4	0.3,-3.3	3.7,-24.8	0.3,-3.1
N16	0.6,1.5	0.6,2.7	1.2,-3	0.7,-0.6	1.8,4.3	2.7,4.4	-0.1,2.2	2.7,-18.5	0.2,-3.3	3.5,-24.9	0.2,-3.2
N17	0.7,1.3	0.7,2.5	1.3,-3.1	0.8,-0.7	1.8,4.1	2.8,4.2	0.2	2.8,-18.6	0.3,-3.4	3.6,-25.1	0.3,-3.3
N18	0.6,1.2	0.6,2.4	1.2,-3.3	0.7,-0.8	1.7,4	2.7,4.1	-0.1,1.9	2.7,-18.8	0.2,-3.6	3.5,-25.2	0.1,-3.5
N19	0.7,1.2	0.6,2.4	1.2,-3.3	0.7,-0.8	1.8,4	2.7,4.1	-0.1,1.9	2.8,-18.8	0.2,-3.6	3.5,-25.2	0.2,-3.5
Met	0.8,1.5	0.7,2.7	1.3,-3	0.8,-0.6	1.9,4.3	2.8,4.4	0.2,2	2.9,-18.5	0.3,-3.3	3.6,-24.9	0.3,-3.2

	N10	N11	N12	N14	N15	N16	N17	N18	N19	Met
5TM	0.6,19.1	0.2,10.9	0.4,11	0.9,8	0.2,6.1	-0.1,6.7	0.1,5.9	-0.1,6.2	-0.1,5.8	0.5,8
7ETM+	0.9,20.1	0.5,12	0.6,12.2	0.3,10.9	0.3,7.3	0.1,8	0.2,7.2	0.1,7.4	0.1,7	0.2,7.1
VGT1	-0.1,15.9	-0.2,7.4	-0.1,7.5	-0.4,6.2	-0.1,2.4	-0.4,3.1	-0.2,2.2	-0.3,2.5	-0.3,2.1	-0.2,2.1
VGT2	0.2,17.6	0,9.2	0.1,9.4	-0.2,8.1	0,4.3	-0.3,5	-0.1,4.1	-0.2,4.4	-0.2,4	-0.1,4.1
MS	2.5,19.9	1.9,11.8	2.1,11.9	1.7,10.7	1.6,7	1.3,7.7	1.5,6.9	1.3,7.2	1.3,6.8	1.5,6.8
MR	3.2,22.3	2.8,14.4	2.9,14.5	2.6,13.3	2.6,9.8	2.4,10.4	2.5,9.6	2.4,9.9	2.4,9.5	2.5,9.6
MD	0.6,20.5	0.3,12.4	0.4,12.5	0.1,11.3	0.2,7.7	0.8,3	0.1,7.5	0.7,8	0.7,4	0.1,7.4
N6	0.3,-1.4	0.3,-11.8	0.5,-11.5	0.1,-13.1	0.7,-17.8	0.3,-17	0.6,-18	0.5,-17.7	0.5,-18.1	0.6,-18.1
N7	0.7,10.5	0.3,1.4	0.5,1.5	0,0.1	0.3,-4	-0.1,-3.2	0.2,-4.1	0,-3.8	0.1,-4.3	0.2,-4.2
N8	0.5,-7.2	0.6,-18.2	0.8,-18	0.4,-19.7	1,-24.6	0.7,-23.7	1,-24.8	0.8,-24.5	0.9,-25	0.9,-24.9
N9	0.7,10.7	0.2,1.6	0.4,1.8	0,0.4	0.2,-3.7	-0.1,-3	0.2,-3.9	0,-3.6	0,-4	0.1,-4
N10		0.1,-10.2	0.3,-10	-0.1,-11.6	0.5,-16.2	0.1,-15.4	0.4,-16.4	0.2,-16.1	0.3,-16.5	0.3,-16.5
N11	2,-10.9		0.2,0.2	-0.2,-1.2	0.1,-5.4	-0.3,-4.6	0,-5.6	-0.1,-5.3	-0.1,-5.7	0,-5.7
N12	1.9,-10.5	-0.1,0.4		-0.4,-1.4	-0.1,-5.6	-0.4,-4.8	-0.2,-5.8	-0.3,-5.5	-0.3,-5.9	-0.2,-5.9
N14	1.9,-12.3	-0.2,-1.2	-0.1,-1.7		0.3,-4.1	0,-3.4	0.3,-4.3	0.1,-4	0.1,-4.4	0.2,-4.4
N15	2.8,-16.7	0.7,-5.2	0.8,-5.6	0.9,-3.9		-0.4,0.7	-0.1,-0.1	-0.3,0.1	-0.2,-0.3	-0.1,-0.2
N16	2.7,-16.8	0.6,-5.2	0.7,-5.7	0.7,-4	-0.2,0		0.3,-0.9	0.1,-0.6	0.2,-1	0.3,-1
N17	2.8,-16.9	0.7,-5.4	0.8,-5.8	0.8,-4.1	-0.1,-0.2	0.1,-0.1		-0.2,0.3	-0.1,-0.1	0,-0.1
N18	2.6,-17.1	0.5,-5.5	0.6,-6	0.7,-4.2	-0.2,-0.3	0,-0.3	-0.1,-0.1		0,-0.4	0.2,-0.4
N19	2.7,-17.1	0.6,-5.5	0.7,-6	0.7,-4.2	-0.2,-0.3	0,-0.3	-0.1,-0.1	0,0		0.1,0
Met	2.8,-16.7	0.7,-5.2	0.8,-5.7	0.9,-3.9	0,0	1,0	0,0.2	0.1,0.3	0.1,0.3	

TABLE VII
SAME AS TABLE IV BUT FOR SWIR REFLECTANCES

	5TM	7ETM+	VGT1	VGT2	MD	N15	N16	N17	N18	N19
5TM		0.4,-4.1	-0.5,-10.4	0.8,-8.3	1.2,-12.8	3.3,-4.5	3.4,-4.1	3.4,-4.4	3.4,-4.3	3,-5.5
7ETM+	0.2,0.3		-1,-6	0.3,-4	0.6,-8.3	2.8,-0.4	2.9,0	2.8,-0.3	2.8,-0.2	2.5,-1.3
VGT1	-0.9,-4.5	-1.1,-4.9		1.2,1.9	1.5,-2.2	3.6,5.3	3.8,5.7	3.7,5.4	3.7,5.5	3.4,4.4
VGT2	0.3,-2.4	0.1,-2.7	1.2,2.1		0.3,-4.1	2.4,3.5	2.6,3.9	2.5,3.6	2.5,3.7	2.2,2.6
MD	0.6,-4.7	0.3,-5.1	1.3,-0.2	0.2,-2.3		2.1,7.3	2.3,7.7	2.2,7.4	2.2,7.5	1.9,6.4
N15	2.7,1.8	2.5,1.5	3.5,6	2.3,4	2.2,6.2		0.1,0.4	0.1,0.1	0.1,0.2	-0.3,-1
N16	2.9,2.2	2.6,1.9	3.6,6.4	2.5,4.4	2.3,6.6	0.1,0.4		-0.1,-0.3	-0.1,-0.2	-0.4,-1.4
N17	2.8,2	2.6,1.7	3.5,6.3	2.4,4.3	2.2,6.4	0.1,0.2	-0.1,-0.2		0,0.1	-0.4,-1.1
N18	2.8,2	2.6,1.8	3.6,6.3	2.4,4.3	2.3,6.5	0.1,0.3	-0.1,-0.1	0,0		-0.4,-1.2
N19	2.4,0.9	2.2,0.6	3.2,5.2	2.3,2	1.9,5.4	-0.3,-0.9	-0.4,-1.3	-0.4,-1.1	-0.4,-1.2	
Met	2.8,2.1	2.6,1.8	3.6,6.3	2.4,4.3	2.3,6.5	0.1,0.3	0,-0.1	0,0.1	0,0	0.4,1.2

values over the entire study area (160 by 160 km) and selected the monthly mean values of the growing seasons for one-on-one comparison and the downscaled NDVI of 16-day MD and 10-day VGT1 and VGT2 for each image scene time profile. Then, the VGT1 and VGT2 were converted to equivalent MD NDVI values based on TOC SRF cross-sensor correction coefficients.

Fig. 5(a) shows the NDVI profile of the sensor systems before SRF cross-sensor correction. The major and perhaps the spurious differences for both original and SRF cross-sensor corrected NDVI values occur during the winter season. This could be due to several factors such as different quality screening methods, varying preferences of pixels for different compositing methods for non vegetated surfaces, and variations of data
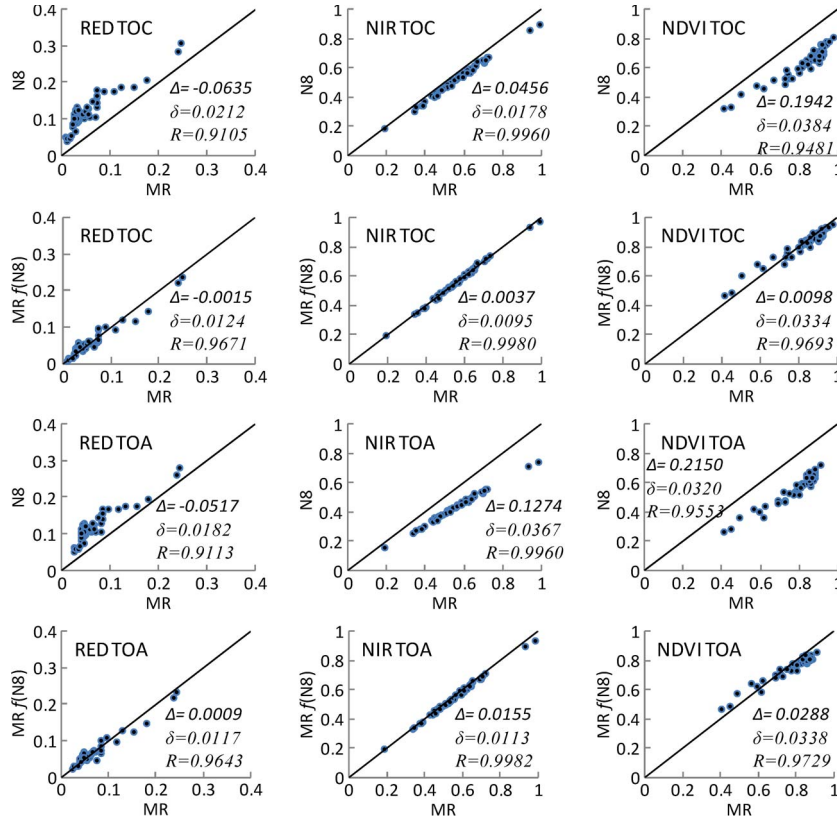
Fig. 4. Variations of red, NIR, and NDVI between AVHRR-1 on NOAA-8 satellite (N8) and MERIS (MR) sensor systems from validation data for top-of-canopy (TOC) and top-of-atmosphere (TOA) values truncated to relevant range of vegetation before and after spectral response function (SRF) cross-sensor correction. This case example shows the worst performance of SRF cross-sensor correction using the (2). Row 1: TOC before SRF cross-sensor correction, row 2: TOC after SRF cross-sensor correction, row 3: TOA before SRF cross-sensor correction, and row 4: TOA after SRF cross-sensor correction. Diagonal is 1 : 1 line. The mean bias (Δ), standard deviation of the bias (δ), and correlation coefficient (R) between the two sensors are also provided.

filling algorithms for missing or contaminated NDVI values. However, for the growing season between April and October (which is the main aim of this study), VGT and MODIS NDVI values varied by mean bias of 4.9% (0.037242) before SRF cross-sensor correction (Fig. 6). The variation is reduced to -0.58% (-0.00436) after NDVI SRF cross-sensor correction (Fig. 6). Unexplained variation can come from several factors as discussed before (Section I). The modeled NDVI from VGT1 and VGT2 sensors follow that of the measured MD NDVI very well [Fig. 5(b)].

VI. COMPARISON WITH PREVIOUS STUDIES

We have established a threshold based on the MAD value whereby the absolute difference of NDVI is less than 0.025 corresponding to bias of within ± 0.025 to be acceptable. This arbitrary threshold is derived from results of [49] on MODIS NDVI accuracy as MODIS is assumed to be the best performing sensor system with on-board radiometric and spectral calibration facility.

Our results agree well with those of [22] and [25] whereby both improving the MAD after SRF cross-sensor correction as does this study (Table VIII). Both [22] and [25] use simple sensor-to-sensor linear least squares regression of $y_{\rm NDIV} = \beta_0 + \beta_1 x_{\rm NDVI}$ form. Steven *et al.* [25] training data were designed to provide a full range of canopy covers, at least two levels of leaf color, a range of soil background brightness and contrasting canopy architectures. Whereas [22] includes

large sets of measured background (soil and snow backgrounds) and leaf spectra as input to SAIL model to simulate canopy spectra for a range of LAI values (simulating different vegetation cover types). The good agreement found between our result and that of [22] and [25] indicates that the training data configuration whereby the use of large dynamics of vegetation range to produce SRF cross-sensor correction is indispensable.

The other two data sets that of [21], [23] and [44] have used similar approach $(x_{\rm NDVI} - y_{\rm NDVI}) = \beta_0 + \beta_1 x_{\rm NDVI} + \beta_2 x_{\rm NDVI^2}$ for developing cross-sensor correction coefficients. The formers used very few measured aircraft observations from the PROBE-1 instrument, whereas [44] used a satellite-based hyperspectral Hyperion image acquired in the dry season in order to develop polynomial cross-sensor correction coefficients of NDVI differences. While the regression approach for SRF cross-sensor correction was analogous to our study, the results in Table VIII indicate that their coefficients may not be applicable for vegetation from other or unknown land cover composition. The main reason for this is that their training data (1) may not represent the large range of vegetation distribution as was aimed in their respective studies, and (2) using air- and spaceborne instruments as a SRF cross-sensor correction training data set may not yield high quality data set due to intrinsic problems in the instrument and measurement operational environments (Section I). Our approach thus provides coefficients for a wide range of bulk SRF cross-sensor correction.

TABLE VIII

MAD, THE MEAN BIAS (Δ), AND STANDARD DEVIATION OF THE BIAS (δ) BASED ON REGRESSION COEFFICIENTS FOUND IN LITERATURE AND THIS STUDY FOR TOC NDVI COMPARISONS. THE MAD, Δ, AND δ BETWEEN THE NDVI OF THE TWO PAIR OF SENSORS ARE ALSO, GIVEN BEFORE SRF CROSS-SENSOR CORRECTION. THE COEFFICIENTS FROM LITERATURE WERE APPLIED ON THE VALIDATION DATA IN THIS STUDY. LIGHT GRAY: MAD $>=$ 0.025

Literature	Sensor y vs. x	Before SRF correction		Literature SRF correction		This study SRF correction	
		MAD	$\Delta(\delta)$	MAD	$\Delta(\delta)$	MAD	$\Delta(\delta)$
Trishchenko et al. [21]	N9 vs.N6	0.0995	0.0995(0.0208)	0.1241	0.1241(0.0222)	0.0200	-0.0165(0.0163)
	N9 vs.N7	0.0008	0.0008(0.0002)	0.0169	0.0169(0.0011)	0.0001	-0.0001(0.0001)
	N9 vs.N8	0.1339	0.1339(0.0262)	0.1240	0.124(0.0253)	0.0242	0.0242(0.019271)
	N9 vs.N10	0.0897	0.0897(0.0205)	0.1164	0.1164(0.0216)	0.0196	-0.0156(0.0165)
	N9 vs.N11	0.0149	0.0149(0.0046)	0.0176	0.0176(0.0047)	0.0044	-0.0026(0.0042)
	N9 vs.N12	0.0181	0.0181(0.0055)	0.0205	0.0205(0.0056)	0.0053	-0.0033(0.005)
	N9 vs.N14	0.0065	0.006(0.0047)	0.0073	-0.0069(0.0046)	0.0051	-0.0038(0.0045)
	N9 vs.N15	0.0241	-0.0241(0.0055)	0.0258	0.0258(0.0065)	0.0047	0.0022(0.0049)
	N9 vs.N16	0.0243	-0.0243(0.005)	0.0224	0.0224(0.0058)	0.0037	0.001(0.0043)
	N9 vs.MD	0.0417	-0.0417(0.0101)	0.0340	0.034(0.0123)	0.0075	0.0015(0.0093)
Trishchenko [23]	N9 vs. N17	0.0255	-0.0255(0.0059)	0.0234	0.0234(0.0066)	0.0047	0.0016(0.0053)
	N9 vs. N18	0.0265	-0.0265(0.0062)	0.0257	0.0257(0.0073)	0.0045	0.0008(0.0055)
	N9 vs. Met	0.0243	-0.0243(0.0054)	0.0213	0.0213(0.0051)	0.0044	0.0019(0.0047)
	N18 vs. N15	0.0024	0.0024(0.0009)	0.0007	0.0004(0.0009)	0.0015	0.0015(0.0008)
	N18 vs. N16	0.0024	0.0022(0.0016)	0.0034	-0.0034(0.0018)	0.0012	0.0003(0.0017)
	N18 vs. N17	0.0010	0.001(0.0004)	0.0025	-0.0025(0.0008)	0.0008	0.0008(0.0004)
	N18 vs. Met	0.0022	0.0022(0.001)	0.0049	-0.0047(0.0031)	0.0013	0.0012(0.0009)
van Leeuwen et al. [22]	N16 vs. MD	0.0175	0.0175(0.0057)	0.0080	0.0064(0.0065)	0.0044	0.0004(0.0058)
	N14 vs. MD	0.0478	0.0478(0.0139)	0.0177	0.0153(0.0141)	0.0111	0.0056(0.0131)
Steven et al. [25]	TM vs. ETM+	0.0098	-0.0098(0.0037)	0.0059	0.0055(0.0039)	0.0027	0.0004(0.0035)
	TM vs. MD	0.0061	-0.0056(0.0049)	0.0058	0.0048(0.0049)	0.0066	0.0058(0.0051)
	TM vs. MS	0.0235	-0.0235(0.0112)	0.0184	0.0167(0.0117)	0.0100	-0.008(0.011)
	TM vs. MR	0.0242	-0.0242(0.0105)	0.0198	0.0183(0.0121)	0.0149	-0.0147(0.0101)
	ETM+ vs. MD	0.0053	0.0042(0.0049)	0.0046	-0.0016(0.0054)	0.0065	0.0055(0.005)
	ETM+ vs. MS	0.0137	-0.0137(0.008)	0.0132	0.0117(0.0084)	0.0094	-0.0088(0.008)
	ETM+ vs. MR	0.0144	-0.0143(0.0087)	0.0142	0.0123(0.0097)	0.0156	-0.0156(0.0084)
	MD vs. MS	0.0184	-0.0179(0.0118)	0.0165	0.0138(0.0126)	0.0139	-0.0128(0.0119)
	MD vs. MR	0.0190	-0.0186(0.013)	0.0182	0.0145(0.0144)	0.0141	-0.0193(0.0132)
	MS vs. MR	0.0043	-0.0006(0.0056)	0.0039	0.0007(0.0055)	0.0079	-0.007(0.0058)
Miura et al. [44]	MD vs. N14	0.0478	0.0478(0.0139)	0.0513	-0.0513(0.0166)	0.0111	-0.0041(0.0133)
	MD vs. ETM+	0.0053	-0.0042(0.0049)	0.0108	-0.0028(0.0138)	0.0060	-0.0051(0.005)
	ETM+ vs. N14	0.0520	0.052(0.0163)	0.0570	-0.0562(0.0322)	0.0118	0.0021(0.0161)

VII. POTENTIAL APPLICATIONS AND LIMITATIONS

The SRF cross-sensor correction analyses presented here were limited to the application for global vegetation conditions and common atmospheric states. The TOC SRF cross-sensor correction coefficients can be used for long-term regional and global monitoring of vegetation using 8 or more days of reflectance composites. This is in line with historical and current archiving of coarse resolution satellite data sets such as SPOT VGT, MODIS, and MERIS for which atmospheric corrections are performed and data sets are composited using a minimum of 8 days reflectances. Wavelength-dependent factors such as aerosol variability and BRDF can affect the accurate use of the TOA SRF cross-sensor correction approaches presented here. However, it can be argued that most application of coarse resolution satellite data sets relies on atmospherically corrected time series composites. Additionally, once the satellite data sets are corrected for atmospheric effects, the TOC SRF cross-sensor correction coefficients can be used instead of the use of TOA coefficients priori to atmospheric corrections. Although previous studies have addressed the problem of SRF cross-sensor corrections (e.g., [15], [16], [21]–[26]), one can argue that the use of the previous results has been limited to
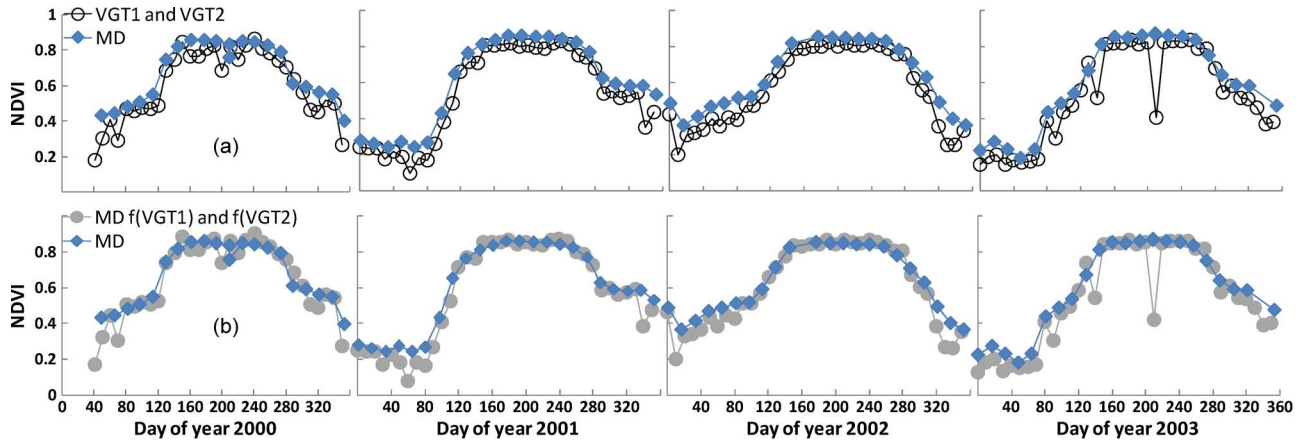
Fig. 5. Multitemporal scene-averaged NDVI profile from the SPOT VEGETATION (VGT1 and VGT2) and MODIS Terra (MD over Harvard Forest. (a) Original NDVI profile and (b) NDVI profile after spectral response function cross-sensor correction between MD and VGT1/VGT2.
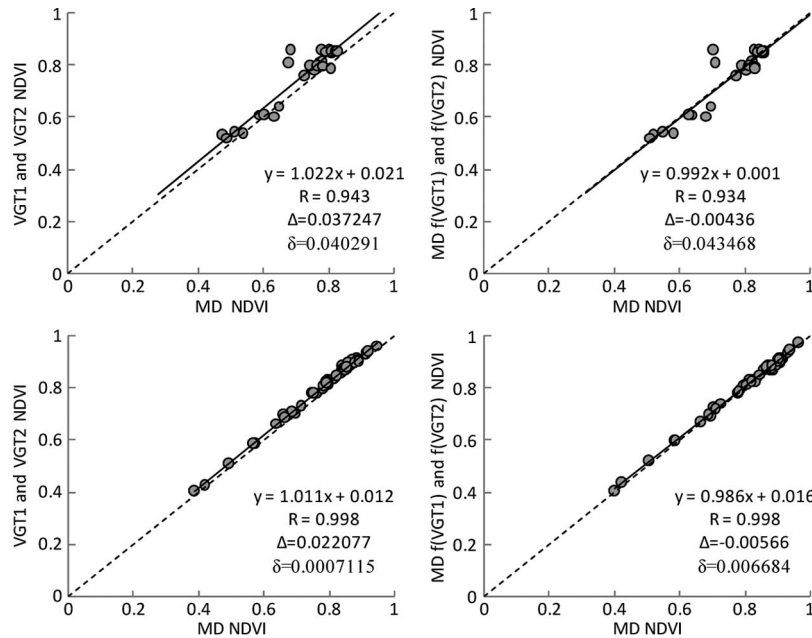

Fig. 6. Variations of NDVI between SPOT VEGETATION (VGT1 and VGT2) plotted against the corresponding value of MODIS Terra (MD) from mean monthly growing season measured satellite data before spectral response function (SRF) cross-sensor correction (Row 1 left), and after SRF cross-sensor correction (Row 1 right). Row 2 left: before SRF cross-sensor correction from measured top-of-canopy validation data. Row 2 right: after SRF cross-sensor correction from measured top-of-canopy validation data. The mean bias (Δ), standard deviation of the bias (δ), and correlation coefficient (R) are also provided. Broken diagonal is 1 : 1 line.

SRF cross-sensor coefficient generation data sets, or geographic regions. It should be acknowledged to this regard that we have used larger spectral information and representative training data sets in regression coefficients in order to remove these limitations. Currently, the SRF cross-sensor correction coefficients developed here are successfully applied in generating long-term leaf area index products in GLOBCARBON physically based LAI algorithm by using a combination of data sets from Landsat TM5, MODIS, and SPOT VGT [50]. The SRF cross-sensor correction coefficients can be used for a number of applications ranging from long-term vegetation phenology studies, generation of large-scale biophysical and biochemical parameters (e.g., leaf area index, fAPAR, chlorophyll), and monitoring land surface moisture particularly using the SWIR spectral bands. Historical products such as AVHRR NDVI time series can also be converted to recent satellite missions with careful correction of satellite orbital drifts. In addition to the ob-

vious limitations of our SRF cross-sensor correction approach as discussed in previous sections (Sections I and II-E), the scope of this research does not include the individual or combined effects of sensor calibration accuracy, scanning and sampling systems, BRDF, and atmospheric variability for cross-sensor reflectance or NDVI corrections.

VIII. CONCLUSION

Large-scale vegetation assessment strategies are increasingly incorporating spaceborne remotely sensed information to monitor current and historical vegetation dynamics and often rely on the combined use of multisensor data due to the relatively short life span of satellite sensors. Practical and operational uses of satellite reflective data to aid our understanding of changing environment must be based on a quantitative appreciation of the uncertainty between different data sources. SRF, describing

the relative sensitivity of the sensor to different wavelengths, has been recognized as one of the most important uncertainty sources for comparability of multisensor monitoring of global vegetation. Twenty-one Earth observation satellite sensors which are relevant for historical and global studies of vegetation were considered for SRF cross-sensor correction. Our SRF cross-sensor correction approach was found to be robust through including the polynomial regression and spectral curve information derived from red and NIR reflectances generated from a large data set representing a wide dynamics of vegetation distributions to minimize land cover specific SRF correction coefficient variations. This new SRF cross-sensor correction approach was evaluated based on independent ground measurements, real satellite data, and previous studies. This study not only provides SRF cross-sensor correction approach, it also highlights the differences of red, NIR, SWIR, and NDVI from various satellites due to SRF variations.

The implications of this study are that reflectances and NDVI from different satellite sensors cannot be regarded as directly equivalent. SRF cross-sensor correction coefficients from this study can nevertheless be applied on any land cover types aimed at extracting vegetation information, and are better suited for prevalently vegetated than bare surfaces. For the red band, sensor systems with the most narrow bandwidth (e.g., MS, MR, MD) which avoids the red-edge, and with the most broad bandwidth (e.g., N6, N8, N10) which overlaps with the red-edge, are the most incomparable to each other. The major SRF variation arises from the overlap of red and NIR bands with the red-edge, while the red band is the most incomparable spectral region due to SRF variations among sensor systems. This incomparability is however reduced from 33.9% (20.1%) to 9.4% (6%) after applying the SRF cross-sensor correction coefficients on independent top of canopy (top of atmosphere) data for all-embraced-sensor comparisons. All AVHRR-3 data can be used without SRF cross-sensor correction. TOA SRF cross-sensor correction coefficients can be used to TOA data of a single day or short interval composites. However, for 10 days or longer composites, the TOC SRF cross-sensor correction coefficients perform better. All the SRF cross-sensor correction presented in this study should be interpreted as bulk SRF cross-sensor correction which particularly for NDVI will significantly improve the comparability of data set from various sensors. The results from this study provides novel opportunities for monitoring crops through the growing season and better continuity of long-term monitoring of vegetation responses to environmental change.

Both TOC and TOA SRF cross calibration coefficients can be obtained by email to the second author or at http://ortelius.geog.utoronto.ca/data/Research/chenres/SRF_cross_sensor_coefficient.pdf.

References

[1] P. J. Sellers, C. J. Tucker, G. J. Collatz, S. O. Los, C. O. Justice, D. A. Dazlich, and D. A. Randall, "A global 1 degree by 1 degree NDVI data set for climate studies. Part 2: The generation of global fields of terrestrial biophysical parameters from the NDVI," *Int. J. Remote Sens.*, vol. 15, no. 17, pp. 3519–3545, Nov. 20, 1994.

[2] C. Tucker, J. Pinzon, M. Brown, D. Slayback, E. Pak, R. Mahoney, E. Vermote, and N. El Saleous, "An extended AVHRR 8-km NDVI dataset compatible with MODIS and SPOT vegetation NDVI data," *Int. J. Remote Sens.*, vol. 26, no. 20, pp. 4485–4498, Oct. 20, 2005.

[3] K. B. Kidwell, *NOAA Polar Orbiter Data, TIROS-N, NOAA-6, NOAA-7, NOAA-8, NOAA-9, NOAA-10, NOAA-11, NOAA-12 Users Guide; NOAA/NESDIS, 1991* , 1991, NOAA/NESDIS.

[4] A. J. Peters, E. A. Walter-Shea, L. Ji, A. Vliia, M. Hayes, M. D. Svoboda, and R. E. D. Nir, "Drought monitoring with NDVI-based standardised vegetation index," *Photogram. Eng. Remote Sens.*, vol. 68, no. 1, pp. 71–75, Jan. 2002.

[5] A. Kawabata, K. Ichii, and Y. Yamaguchi, "Global monitoring of the interannual changes in vegetation activities using NDVI and its relationships to temperature and precipitation," *Int. J. Remote Sens.*, vol. 22, no. 7, pp. 1377–1382, 2001.

[6] N. Pettorelli, J. O. Vik, A. Mysterud, J.-M. Gaillard, C. J. Tucker, and N. C. Stenseth, "Using the satellite-derived NDVI to assess ecological responses to environmental change," *Trends Ecol. Evol.*, vol. 20, no. 9, pp. 503–510, Sep. 2005.

[7] M. E. James and S. N. V. Kalluri, "The pathfinder AVHRR land dataset: An improved coarse resolution dataset for terrestrial monitoring," *Int. J. Remote Sens.*, vol. 15, no. 17, pp. 3347–3363, 1994.

[8] H. Ouaidrari, N. El Saleous, E. F. Vermote, J. R. Townshend, and S. N. Goward, "AVHRR Land Pathfinder II (ALP II) data set: Evaluation and inter-comparison with other data sets," *Int. J. Remote Sens.*, vol. 24, no. 1, pp. 135–142, Jan. 10, 2003.

[9] S. O. Los, G. J. Collatz, P. J. Sellers, C. M. Malmström, N. H. Pollack, R. S. DeFries, L. Bounoua, M. T. Parris, C. J. Tucker, and D. A. Dazlich, "A global 9-yr biophysical land surface dataset from NOAA AVHRR data," *J. Hydrometeorol.*, vol. 1, no. 2, pp. 183–199, Apr. 2000.

[10] J. L. Privette, C. Fowler, G. A. Wick, J. Yang, and M. Markham, "Effects of orbital drift on advanced very high resolution radiometer products: Normalized difference vegetation index and sea surface temperature," *Remote Sens. Environ.*, vol. 53, no. 3, pp. 164–171, Sep. 1995.

[11] P. D'Odorico, L. Guanter, M. E. Schaepman, and D. Schläpfer, "Performance assessment of onboard and scene-based methods for airborne prism experiment spectral characterization," *Appl. Opt.*, vol. 50, no. 24, pp. 4755–4764, Aug. 20, 2011.

[12] R. E. Wolfe, M. Nishihama, A. J. Fleig, J. A. Kuyper, D. P. Roy, J. C. Storey, and F. S. Patt, "Achieving sub-pixel geolocation accuracy in support of MODIS land science," *Remote Sens. Environ.*, vol. 83, no. 1–2, pp. 31–49, Nov. 2002.

[13] P. M. Teillet, K. Staenz, and D. J. Williams, "Effects of spectral, spatial, radiometric characteristics on remote sensing vegetation indexes of forested regions," *Remote Sens. Environ*, vol. 61, no. 1, pp. 139–149, Jul. 1997.

[14] P. M. Teillet, G. Fedosejevs, R. P. Gauthier, N. T. O'Neill, K. J. Thome, S. F. Biggar, H. Ripley, and A. Meygret, "A generalized approach to the vicarious calibration of multiple Earth observation sensors using hyperspectral data," *Remote Sens. Environ.*, vol. 77, no. 3, pp. 304–327, Sep. 2001.

[15] P. M. Teillet, G. Fedosejevs, K. J. Thome, and J. L. Barker, "Impacts of spectral band difference effects on radiometric cross-calibration between satellite sensors in the solar-reflective spectral domain," *Remote Sens. Environ.*, vol. 110, no. 3, pp. 393–409, Oct. 15, 2007.

[16] P. M. Teillet, B. L. Markham, and R. R. Irish, "Landsat cross-calibration based on near simultaneous imaging of common ground targets," *Remote Sens. Environ.*, vol. 102, no. 3/4, pp. 264–270, Jun. 15, 2006.

[17] K. Y. Kondratyev, V. V. Kozoderov, and O. I. Smokty, *Remote Sensing of the Earth From Space: Atmospheric Correction*. Heidelberg, Germany: Springer-Verlag, 1992.

[18] E. F. Vermote, D. Tanre, J. L. Deuze, M. Herman, and J. J. Morcette, "Second simulation of the satellite signal in the solar spectrum, 6 S: An overview," *IEEE Trans. Geosci. Remote Sens.*, vol. 35, no. 3, pp. 675–686, May 1997.

[19] S. Liang, A. H. Strahler, M. J. Barnsley, C. C. Borel, S. A. W. Gerstl, D. J. Diner, A. J. Prata, and C. L. Walthall, "Multiangular remote sensing past, present and future," *Remote Sens. Rev.*, vol. 18, no. 2–4, pp. 83–102, 2000.

[20] D. J. Meyer, "Estimating the effective spatial resolution of an AVHRR time series," *Int. J. Remote Sens.*, vol. 17, no. 15, pp. 2971–2980, Oct. 1996.

[21] A. P. Trishchenko, J. Cihlar, and Z. Q. Li, "Effects of spectral response function on surface reflectance and NDVI measured with moderate resolution satellite sensors," *Remote Sens. Environ.*, vol. 81, no. 1, pp. 1–18, Jul. 2002.

[22] W. J. D. van Leeuwen, B. J. Orr, S. E. Marsh, and S. M. Herrmann, "Multi-sensor NDVI data continuity: Uncertainties and implications for vegetation monitoring applications," *Remote Sens. Environ.*, vol. 100, no. 1, pp. 67–81, Jan. 15, 2006.

[23] A. P. Trishchenko, "Effects of spectral response function on surface reflectance and NDVI measured with moderate resolution satellite sensors: Extension to AVHRR NOAA-17,18 and METOP-A," *Remote Sens. Environ.*, vol. 113, no. 2, pp. 335–341, Feb. 16, 2009.

[24] P. M. Teillet and X. Ren, "Spectral band difference effects on vegetation indices derived from multiple satellite sensor data," *Can. J. Remote Sens.*, vol. 34, no. 3, pp. 159–173, Aug. 2008.

[25] M. D. Steven, T. J. Malthus, F. Baret, H. Xu, and M. J. Chopping, "Inter-calibration of vegetation indices from different sensor systems," *Remote Sens. Environ.*, vol. 88, no. 4, pp. 412–422, Dec. 30, 2003.

[26] C. R. N. Rao, C. Cao, and N. Zhang, "Inter-calibration of the moderate-resolution imaging spectroradiometer and the AlongTrack scanning radiometer-2," *Int. J. Remote Sens.*, vol. 24, no. 9, pp. 1913–1924, May 10, 2003.

[27] T. Cocks, R. Jenssen, A. Stewart, I. Wilson, and T. Shields, "The HyMap Airborne Hyperspectral Sensor: The System, Calibration and Performance," presented at the 1st EARSEL Workshop Imaging Spectroscopy, Zurich, Switzerland, 1998.

[28] GCOS, *Implementation Plan for the Global Observing System for Climate in Support of the UNFCCC*, p. 180 , 2010, GCOS-138 (GOOS-184, GTOS-76, WMO-TD/No. 152).

[29] P. Ceccato, S. Flasse, S. Tarantola, S. Jacquemoud, and J.-M. Grégoire, "Detecting vegetation leaf water content using reflectance in the optical domain," *Remote Sens. Environ.*, vol. 77, no. 1, pp. 22–33, Jul. 2001.

[30] L. Brown, J. M. Chen, S. G. Leblanc, and J. Cihlar, "A shortwave infrared modification to the simple ratio for LAI retrieval in boreal forests: An image and model analysis," *Remote Sens. Environ.*, vol. 71, no. 1, pp. 16–25, Jan. 2000.

[31] F. Deng, J. M. Chen, S. Plummer, M. Chen, and J. Pisek, "Algorithm for global leaf area index retrieval using satellite imagery," *IEEE Trans. Geosci. Remote Sens.*, vol. 44, no. 8, pp. 2219–2229, Aug. 2006.

[32] S. Jacquemoud and F. Baret, "PROSPECT: A model of leaf optical properties," *Remote Sens. Environ.*, vol. 34, no. 2, pp. 75–91, Nov. 1990.

[33] W. Verhoef, "Light scattering by leaf layers with application to canopy reflectance modeling: The SAIL model," *Remote Sens. Environ.*, vol. 16, no. 2, pp. 125–141, Oct. 1984, 1984.

[34] S. Jacquemoud, W. Verhoef, F. Baret, C. Bacour, P. J. Zarco-Tejada, G. P. Asner, C. François, and S. L. Ustin, "PROSPECT plus SAIL models: A review of use for vegetation characterization," *Remote Sens. Environ.*, vol. 113, pp. S56–S66, Sep. 2009.

[35] W. Verhoef and H. Bach, "Coupled soil-leaf-canopy and atmosphere radiative transfer modeling to simulate hyperspectral multi-angular surface reflectance and TOA radiance data," *Remote Sens. Environ.*, vol. 109, no. 2, pp. 166–182, Jul. 30, 2007.

[36] R. Latifovic, J. Cihlar, and J. Chen, "A comparison of BRDF models for the normalization of satellite optical data to a standard sun-target-sensor geometry," *IEEE Trans. Geosci. Remote Sens.*, vol. 41, no. 8, pp. 1889–1898, Aug. 2003.

[37] G. Fedosejevs, N. O'Neill, A. Royer, P. M. Teillet, A. I. Bokoye, and B. McArthur, "Aerosol optical depth for atmospheric correction of AVHRR composite data," *Can. J. Remote Sens.*, vol. 26, no. 4, pp. 273–284, 2000.

[38] A. M. Baldridge, S. J. Hook, C. I. Grove, and G. Rivera, "The ASTER spectral library version 2.0," *Remote Sens. Environ.*, vol. 113, no. 4, pp. 711–715, Apr. 15, 2009.

[39] R. N. Clark, G. A. Swayze, R. Wise, E. Livo, T. Hoefen, R. Kokaly, and S. J. Sutley, *USGS Digital Spectral Library splib06a* , U.S. Geological Survey, 2007, Digital Data Series 231.

[40] B. Yoder and L. Johnson, "Seedling canopy reflectance spectra, 1992–1993 accelerated canopy chemistry program (ACCP)," Oak Ridge Nat. Lab. Distrib. Active Archive Center, Oak Ridge, TN, 1999.

[41] M. Helmlinger, W. Buermann, and F. Eckardt, "SAFARI 2000 surface spectral reflectance at Sua Pan, Botswana, dry season 2000," Oak Ridge Nat. Lab. Distrib. Active Archive Center, Oak Ridge, TN, 2005.

[42] B. L. Markham, J. C. Storey, D. L. Williams, and J. R. Irons, "Landsat sensor performance: History and current status," *IEEE Trans. Geosci. Remote Sens.*, vol. 42, no. 12, pp. 2691–2694, Dec. 2004.

[43] K. Gallo, L. Li, B. Reed, J. C. Eidenshink, and J. L. Dwyer, "Multi-platform comparisons of MODIS and AVHRR normalized difference vegetation index data," *Remote Sens. Environ.*, vol. 99, no. 3, pp. 221–231, Nov. 30, 2005.

[44] T. Miura, A. Huete, and H. Yoshioka, "An empirical investigation of cross-sensor relationships of NDVI and red/near-infrared reflectance using EO-1 hyperion data," *Remote Sens. Environ.*, vol. 100, no. 2, pp. 223–236, Jan. 30, 2006.

[45] P. D'Odorico, E. Alberti, and M. E. Schaepman, "In-flight spectral performance monitoring of the airborne prism experiment," *Appl. Opt.*, vol. 49, no. 16, pp. 3082–3091, Jun. 1, 2010.

[46] R. Fensholt, K. Rasmussen, T. T. Nielsen, and C. Mbow, "Evaluation of earth observation based long term vegetation trends—Intercomparing NDVI time series trend analysis consistency of Sahel from AVHRR GIMMS, Terra MODIS and SPOT VGT data," *Remote Sens. Environ.*, vol. 113, no. 9, pp. 1886–1898, Sep. 2009.

[47] E. Tarnacsky, S. Garrigues, and M. E. Brown, "Multiscale geostatistical analysis of AVHRR, SPOT-VGT and MODIS global NDVI products," *Remote Sens. Environ.*, vol. 112, no. 2, pp. 535–549, Feb. 2008.

[48] A. Gonsamo, "Leaf area index retrieval using gap fractions obtained from high resolution satellite data: Comparisons of approaches, scales and atmospheric effects," *Int. J. Appl. Earth Obs.*, vol. 12, no. 4, pp. 233–248, Aug. 2010.

[49] X. Gao, A. R. Huete, and K. Didan, "Multisensor comparisons and validation of MODIS vegetation indices at the semiarid Jornada experimental range," *IEEE Trans. Geosci. Remote Sens*, vol. 41, no. 10, pp. 2368–2381, Oct. 2003.

[50] A. Gonsamo and J. M. Chen, "Improved LAI algorithm implementation to MODIS data by incorporating background, topography and foliage clumping information," *IEEE Trans. Geosci. Remote Sens.*, submitted for publication.

Alemu Gonsamo received the B.Sc. degree (distinction) in forestry at Wondo Genet College of Forestry, Debub University, Awassa, Ethiopia, in 2002, the M.Sc. degree in geo-information science from Wageningen University, Wageningen, The Netherlands, in 2006, and the Ph.D. degree in geography from the University of Helsinki, Espoo, Finland, in 2009.

From 2002 to 2004, he worked as a Graduate Assistant and Academic Coordinator. In 2010, he was a Postdoctoral Fellow at the Department of Geography and Geosciences. Currently, he is a Postdoctoral Fellow with the University of Toronto, Toronto, ON. His recent research interests are in the remote sensing of biogeophysical parameters, plant canopy radiation modeling, optical satellite sensor cross calibration, remote sensing of plant phenology, and territorial carbon cycle modeling.

Jing M. Chen received the B.Sc. degree in applied meteorology from the Nanjing Institute of Meteorology, Nanjing, China, in 1982, and the Ph.D. degree in meteorology from Reading University, Reading, U.K., in 1986. From 1989 to 1993, he was a Postdoctoral Fellow and Research Associate with the University of British Columbia, Vancouver, BC, Canada.

From 1993 to 2000, he was a Research Scientist with the Canada Center for Remote Sensing, Ottawa, ON, Canada. Currently, he is a Professor with the University of Toronto, Toronto, ON, Canada, and an Adjunct Professor with York University, Toronto. He has published over 200 papers in refereed journals. His recent research interests are in the remote sensing of biophysical parameters, plant canopy radiation modeling, terrestrial water and carbon cycle modeling, and atmospheric inverse modeling for global and regional carbon budget estimation.

Dr. Chen is a Fellow of the Royal Society of Canada and a Senior Canada Research Chair. He served as an Associate Editor of the IEEE TRANSACTIONS ON GEOSCIENCE AND REMOTE SENSING from 1996 to 2002.